Int J Adv Manuf Technol (2017) 91:4313–4330
DOI 10.1007/s00170-017-0067-x

ORIGINAL ARTICLE

Orthogonal polynomial approximation method for stability prediction in milling

Zhenghu Yan[1] · **Xibin Wang**[1] · **Zhibing Liu**[1] · **Dongqian Wang**[1] · **Yongjian Ji**[1] · **Li Jiao**[1]

Received: 31 August 2016 / Accepted: 16 January 2017 / Published online: 13 February 2017

Abstract Based on orthogonal polynomial approximation scheme, this paper presents several stability prediction methods using different kinds of orthogonal polynomials. The milling dynamics with consideration of the regenerative effect is described by time periodic delay-differential equations (DDEs). Firstly, this work employs the classical Legendre and Chebyshev polynomials to approximate the state term, delayed term, and periodic-coefficient matrix. With the help of direct integration scheme (DIS), the state transition matrixes which indicate the mapping relations of the dynamic response between the current tooth pass and the previous tooth pass are obtained. The stability lobe diagrams for single degree of freedom (DOF) and two DOF milling models are generated by using the Legendre and Chebyshev polynomial approximation-based methods. The rate of convergence of the Legendre and Chebyshev polynomial-based methods is compared with that of the benchmark first-order semi-discretization method (1stSDM). The comparison results indicate that the rate of convergence and the numerical stability of the Legendre and Chebyshev polynomial-based methods are both need to be improved. In order to develop new methods with high rate of convergence and numerical stability base on DIS, the monic orthogonal polynomial sequences are constructed by using Gram-Schmidt orthogonalization to approximate the state term, delayed term, and periodic-coefficient matrix. The rate of convergence and the computational efficiency of the monic orthogonal polynomial-based methods are evaluated by comparing with those of the benchmark 1stSDM. The results turn out that the monic orthogonal polynomial-based methods are advantageous in terms of the rate of convergence and numerical stability. The stability lobe diagrams for single DOF and two DOF milling models obtained by the monic orthogonal polynomial-based methods are compared with those obtained by the 1stSDM. Finally, the monic orthogonal polynomial-based methods are proved to be the effective and efficient methods to predict the milling stability.

Keywords Orthogonal polynomials · Stability prediction · Regenerative effect · The rate of convergence · Numerical stability

1 Introduction

In milling process, regenerative chatter is an undesirable self-excited vibration between cutting tool and workpiece. It refers to the unstable phenomenon that a wavy surface left behind by previous tooth is removed by current tooth [1]. Chatter may cause poor surface finish, accelerated tool wear, and even accelerated machine tool wear [2]. As many literatures mentioned, regenerative chatter is one of the most common obstacles to achieve high-performance milling operations. To gain desirable surface finish, proper parameters should be selected for milling operations. Stability lobe diagrams which indicate the relations between the axial depth of cut and the spindle speed of the machine tool are available for selecting proper parameters.

The mathematical models of milling dynamics with consideration of the regenerative effect can be described as time periodic delay-differential equations (DDEs). Based on the DDEs, different methods for chatter stability prediction in milling have been developed. Altintas et al. [3] proposed a

✉ Zhibing Liu
liuzhibing@bit.edu.cn

[1] Key Laboratory of Fundamental Science for Advanced Machining, School of Mechanical Engineering, Beijing Institute of Technology, Beijing 100081, China

zeroth-order approximation (ZOA) method which employs Fourier series to approximate dynamic cutting force coefficients. In this method, the axial depth of cut and the spindle speed are calculated by using real and image part of the characteristic equation of the system in frequency domain. On the basis of ZOA method, Merdol et al. [4] presented a multi-frequency method which utilizes higher order harmonics of the Fourier series expansion to approximate the dynamic cutting force coefficients. Shorr et al. [5] established a compliance feedback model which describes the dynamic behavior of regenerative chatter for tool-workpiece interaction. Li et al. [6] presented a time domain method for chatter stability analysis in milling. In this method, the ratio of the predicted maximum dynamic cutting force to the predicted maximum static cutting force is used as a criterion for chatter stability analysis. Tangjitsitcharoen et al. [7] developed an in-process detection method for predicting chatter in milling processes. In this method, the average variances of the dynamic cutting forces of three force components are employed to identify the chatter. Bayly et al. [8] reported a temporal finite element analysis method, which is based on the use of multiple finite elements in the time domain. Butcher et al. [9] suggested the Chebyshev collocation method. In this method, the derivatives of functions are approximated by introducing the spectral differentiation matrix. Xie et al. [10] developed an improved complete dicretization method to predict milling stability. In this method, most of the differential terms are discretized with Euler's method. Insperger and Stépán proposed the zeroth-order semi-discretization method (othSDM) [11] and first-order semi-discretization method (1stSDM) [12] which respectively use the zeroth-order and first-order piecewise constant function to approximate the delayed term. These two semi-discretization methods are widely used to predict the stability in milling.

With the aim of improving the computational efficiency for obtaining the stability lobe diagram, Ding et al. [13] presented a full-discretization method (FDM) based on the DIS. Then, different methods based on the DIS are proposed. Ding et al. developed the second-order FDM [14] and numerical integration method [15] to calculate the stability boundary of the milling process. Liang et al. [16] reported an improved numerical integration method and extended this method to low radial immersion milling condition where varying time delay has to be considered. Guo et al. [17] suggested a third-order FDM for predicting the milling stability. Ozoegwu [18] reported a least-squares approximation method to obtain the milling stability lobe diagrams. Compared with the semi-discretization methods, the DIS-based methods are not only able to improve the computational efficiency, but also can promote the rate of convergence which reflects the computational accuracy of prediction method.

Additionally, the key point of milling stability prediction is to solve the DDEs for achieving the mapping relations of the dynamic response between the current tooth pass and the previous tooth pass. Orthogonal polynomials can be effectively used to solve differential equations. Villadsen et al. [19] employed orthogonal polynomials to solve computational problems in linear and nonlinear ordinary differential equations. Funaro [20] adopted the orthogonal polynomials to solve ordinary differential equations and time-dependent problems. In this paper, different orthogonal polynomials are used to solve the time periodic DDEs of milling process in the framework of DIS. The motivation of this study is to solve the DDEs using the classical Legendre and Chebyshev polynomials to obtain stability lobe diagrams, and analyze the rate of convergence of these two classical methods. To improve the rate of convergence and numerical stability of the Legendre and Chebyshev polynomial-based methods, the monic orthogonal polynomials which are constructed based on Gram-Schmidt orthogonalization are developed to analyze the milling stability.

The rest of this paper is organized as below. In section 2, the mathematical model of milling process is introduced. In section 3, milling stability analysis based on Legendre and Chebyshev polynomials is presented, and the convergence rate of the Legendre and Chebyshev polynomial-based methods is compared with that of the benchmark lstSDM. In section 4, the monic orthogonal polynomial approximation-based methods are developed to predict the milling stability with the aim of improving the convergence rate. Conclusions are drawn in section 5.

2 Mathematical model of milling process

In this section, the benchmark example for single DOF milling model is studied, as shown in Fig. 1. The governing equation of system motion of a single DOF milling model can be described as [11]

$$\ddot{x}(t) + 2\zeta\omega_n\dot{x}(t) + \omega_n^2 x(t) = -\frac{a_p h(t)}{m}\left(x(t) - x(t-\tau)\right) \tag{1}$$

where ζ is the damping ratio, ω_n is the angular natural frequency, a_p is the axial depth of cut, m is the modal mass, $x(t)$ is the

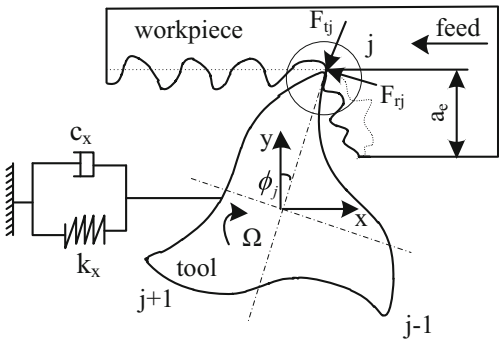

Fig. 1 Dynamic model of the single DOF milling system

displacement in the current tooth pass, $x(t-\tau)$ is the displacement in the previous tooth pass, the time delay τ is equal to the tooth passing period T, and the specific cutting force coefficient $h(t)$ is defined as

$$h(t)=\sum_{j=1}^{N} g\left[\varphi_j(t)\right]\sin\left(\varphi_j(t)\right)\left[K_t\cos\left(\varphi_j(t)\right)+K_n\sin\left(\varphi_j(t)\right)\right] \quad (2)$$

where K_t and K_n are the tangential and the normal cutting force coefficients, respectively, and N is the number of tooth. The angular position of the jth tooth $\varphi_j(t)$ is determined as

$$\varphi_j(t)=\left(2\pi\Omega\Big/60\right)t+(j-1)2\pi\Big/N \quad (3)$$

where Ω denotes the spindle speed in revolutions per minute.

The function $g[\varphi_j(t)]$ is a unit step function which determines whether the tooth is in or out of cut. It is defined as

$$g\left[\varphi_j(t)\right]=\begin{cases}1 & \text{if } \varphi_{st}<\varphi_j(t)<\varphi_{ex}\\ 0 & \text{otherwise}\end{cases} \quad (4)$$

where φ_{st} and φ_{ex} are the start and exit angles of the jth cutter tooth, respectively. For up-milling, $\varphi_{st}=0$ and $\varphi_{ex}=\arccos(1-2a_e/D)$; for down milling, $\varphi_{st}=\arccos(2a_e/D-1)$ and $\varphi_{ex}=\pi$, D is the diameter of cutter, and a_e is the radial depth of cut.

The tangential and the radial cutting force acting on the jth tooth, i.e., F_{tj} and F_{rj}, can be given by

$$F_{tj}=g\left[\varphi_j(t)\right]K_t a_p h_j(t) \quad (5)$$

$$F_{rj}=g\left[\varphi_j(t)\right]K_n a_p h_j(t) \quad (6)$$

Let $\mathbf{x}(t)=\begin{bmatrix}x(t)\\ \dot{x}(t)\end{bmatrix}$; Eq. (1) can be rewritten in the following state space form:

$$\dot{\mathbf{x}}(t)=\mathbf{A}\mathbf{x}(t)+\mathbf{B}(t)\mathbf{x}(t)-\mathbf{B}(t)\mathbf{x}(t-\tau) \quad (7)$$

where $\mathbf{A}=\begin{bmatrix}0 & 1\\ -\omega_n^2 & -2\zeta\omega_n\end{bmatrix}$ is a constant matrix, $\mathbf{B}(t)=\begin{bmatrix}0 & 0\\ -\dfrac{a_p h(t)}{m_t} & 0\end{bmatrix}$ is a periodic-coefficient matrix with $\mathbf{B}(t)=\mathbf{B}(t+T)$.

In order to solve Eq. (7) numerically based on DIS, the first step is to divide the period τ into n equal small time intervals with the length of Δt, that is, $\tau=n\Delta t$, where n is an integer. Equation (7) is integrated on the ith small time interval $[t_i, t_{i+1}]$; the result is

$$\mathbf{x}_{i+1}=e^{\mathbf{A}\Delta t}\mathbf{x}_i+\int_{t_i}^{t_{i+1}} e^{\mathbf{A}(t_{i+1}-s)}[\mathbf{B}(s)\mathbf{x}(s)-\mathbf{B}(s)\mathbf{x}(s-\tau)]\mathrm{d}s \quad (8)$$

With the aim of obtaining the mapping relations of the dynamic response between the current tooth pass and the previous tooth pass, different kinds of orthogonal polynomials are employed to approximate the state term $\mathbf{x}(s)$, delayed term $\mathbf{x}(s\text{-}\tau)$, and periodic-coefficient matrix $\mathbf{B}(s)$ in Eq. (8). Here, Legendre polynomials and Chebyshev polynomials which are two kinds of classical and commonly used orthogonal polynomials are adopted for milling stability analysis.

3 Milling stability analysis based on Legendre and Chebyshev polynomials

Legendre and Chebyshev polynomials are two kinds of classical orthogonal polynomials, which can be used to solve various problems in mathematics and engineering effectively. This section presents the applications of Legendre and Chebyshev polynomials in milling stability analysis based on DIS.

3.1 Milling stability analysis based on Legendre polynomials

Let $L_l(z)$ and $z\in[-1,1]$ be the standard Legendre polynomial of degree l. The shifted Legendre polynomials $L_{T,l}(s)$ and $s\in[a,b]$ are defined as

$$L_{T,l}(s)=L_l\left[\frac{2s-(a+b)}{b-a}\right],\quad l=0,1,2,\cdots. \quad (9)$$

In particular,

$$L_{T,0}(s)=1$$

$$L_{T,1}(s)=\frac{2s-(a+b)}{b-a}$$

$$L_{T,2}(s)=\frac{3}{2}\cdot\left[\frac{2s-(a+b)}{b-a}\right]^2-\frac{1}{2}$$

In Eq. (8), the state term $\mathbf{x}(s)$ can be approximated by the shifted Legendre polynomials as

$$\mathbf{x}(s)=\sum_{k=0}^{l}\mathbf{a}_k\cdot L_{T,k}(s),\quad k\in[0,l] \quad (10)$$

where the coefficient $\mathbf{a}_k$ can be calculated as

$$\mathbf{a}_k=\frac{(\mathbf{x},L_{T,k})}{(L_{T,k},L_{T,k})}=\frac{\sum w_j\mathbf{x}_j L_{T,k}(s_j)}{\sum w_j L^2{}_{T,k}(s_j)} \quad (11)$$

where $\mathbf{x}_j$ is the nodal value of the node s_j, w_j is the weight value, in this paper, and $w_j\equiv 1$.

3.1.1 First-order shifted Legendre polynomial approximation method

In the first-order shifted Legendre polynomial approximation method (1stSLPAM), $L_{T,0}(s)$ and $L_{T,1}(s)$ are adopted to approximate the state term $\mathbf{x}(s)$. The nodes t_i and t_{i+1} and their nodal values $\mathbf{x}_i$ and $\mathbf{x}_{i+1}$ are utilized for calculation. According to Eq. (9), $L_{T,0}(s)$ and $L_{T,1}(s)$ can be represented as

$$L_{T,0}(s) = 1, \quad L_{T,1}(s) = \frac{2s-(t_i + t_{i+1})}{\Delta t} \tag{12}$$

With the substitutions $t_i = 0$ and $t_{i+1} = \Delta t$, Eq. (12) can be rewritten as

$$L_{T,0}(s) = 1, \quad L_{T,1}(s) = \frac{2s}{\Delta t} - 1 \tag{13}$$

On the basis of Eq. (10), the state term $\mathbf{x}(s)$ is obtained as

$$\mathbf{x}(s) = \mathbf{a}_0 L_{T,0}(s) + \mathbf{a}_1 L_{T,1}(s) = \mathbf{a}_0 \cdot 1 + \mathbf{a}_1 \cdot \left(\frac{2s}{\Delta t} - 1\right) \tag{14}$$

where coefficients $\mathbf{a}_0$ and $\mathbf{a}_1$ can be acquired according to Eq. (11) as

$$\mathbf{a}_0 = \frac{\sum_{j=i}^{i+1} w_j \mathbf{x}_j L_{T,0}(s_j)}{\sum_{j=i}^{i+1} w_j L^2{}_{T,0}(s_j)} = \frac{\mathbf{x}_i + \mathbf{x}_{i+1}}{2}, \quad \mathbf{a}_1 = \frac{\sum_{j=i}^{i+1} w_j \mathbf{x}_j L_{T,1}(s_j)}{\sum_{j=i}^{i+1} w_j L^2{}_{T,1}(s_j)} = \frac{-\mathbf{x}_i + \mathbf{x}_{i+1}}{2}$$

The obtained coefficients $\mathbf{a}_0$ and $\mathbf{a}_1$ are inserted to Eq. (14) to become

$$\mathbf{x}(s) = \left(1 - \frac{s}{\Delta t}\right) \cdot \mathbf{x}_i + \frac{s}{\Delta t} \cdot \mathbf{x}_{i+1} \tag{15}$$

Similarly the delayed term $\mathbf{x}(s-\tau)$ and periodic-coefficient matrix $\mathbf{B}(s)$ can be represented as follows:

$$\mathbf{x}(s-\tau) = \left(1 - \frac{s}{\Delta t}\right) \cdot \mathbf{x}_{i-n} + \frac{s}{\Delta t} \cdot \mathbf{x}_{i-n+1} \tag{16}$$

$$\mathbf{B}(s) = \left(1 - \frac{s}{\Delta t}\right) \cdot \mathbf{B}_i + \frac{s}{\Delta t} \cdot \mathbf{B}_{i+1} \tag{17}$$

Substituting Eqs. (15), (16), and (17) into Eq. (8) yields

$$\mathbf{x}_{i+1} = \mathbf{P}_i \begin{bmatrix} (\mathbf{F}_0 + \mathbf{G}_{11}\mathbf{B}_i + \mathbf{G}_{12}\mathbf{B}_{i+1})\mathbf{x}_i - (\mathbf{G}_{12}\mathbf{B}_i + \mathbf{G}_{13}\mathbf{B}_{i+1})\mathbf{x}_{i+1-n} \\ -(\mathbf{G}_{11}\mathbf{B}_i + \mathbf{G}_{12}\mathbf{B}_{i+1})\mathbf{x}_{i-n} \end{bmatrix} \tag{18}$$

where

$$\mathbf{P}_i = [\mathbf{I} - \mathbf{G}_{12}\mathbf{B}_i - \mathbf{G}_{13}\mathbf{B}_{i+1}]^{-1} \tag{19}$$

$$\mathbf{G}_{11} = \frac{1}{(\Delta t)^2}\left[(\Delta t)^2 \cdot \mathbf{F}1 - 2\Delta t \cdot \mathbf{F}2 + \mathbf{F}3\right] \tag{20}$$

$$\mathbf{G}_{12} = \frac{1}{(\Delta t)^2}[\Delta t \cdot \mathbf{F}2 - \mathbf{F}3] \tag{21}$$

$$\mathbf{G}_{13} = \frac{1}{(\Delta t)^2} \cdot \mathbf{F}3 \tag{22}$$

$$\mathbf{F}_0 = e^{\mathbf{A}\Delta t} \tag{23}$$

$$\mathbf{F}_1 = (\mathbf{F}_0 - \mathbf{I})\mathbf{A}^{-1} \tag{24}$$

$$\mathbf{F}_2 = (\mathbf{F}_1 - (\Delta t)\cdot\mathbf{I})\mathbf{A}^{-1} \tag{25}$$

$$\mathbf{F}_3 = \left(2\mathbf{F}_2 - (\Delta t)^2 \cdot \mathbf{I}\right)\mathbf{A}^{-1} \tag{26}$$

$$\mathbf{F}_4 = \left(3\mathbf{F}_3 - (\Delta t)^3 \cdot \mathbf{I}\right)\mathbf{A}^{-1} \tag{27}$$

where $\mathbf{I}$ denotes the identity matrix.

If $\mathbf{P}_i$ is a nonsingular matrix, the local discrete mapping can be expressed as matrix form according to Eq. (18)

$$\begin{Bmatrix} \mathbf{x}_{i+1} \\ \mathbf{x}_i \\ \mathbf{x}_{i-1} \\ \vdots \\ \mathbf{x}_{i+1-n} \end{Bmatrix} = \begin{bmatrix} \mathbf{M}^i_{11} & 0 & \cdots & 0 & \mathbf{M}^i_{1n} & \mathbf{M}^i_{1,n+1} \\ \mathbf{I} & 0 & \cdots & 0 & 0 & 0 \\ 0 & \mathbf{I} & \cdots & 0 & 0 & 0 \\ \vdots & \vdots & \vdots & \vdots & \vdots & \vdots \\ 0 & 0 & 0 & 0 & \mathbf{I} & 0 \end{bmatrix} \begin{Bmatrix} \mathbf{x}_i \\ \mathbf{x}_{i-1} \\ \mathbf{x}_{i-2} \\ \vdots \\ \mathbf{x}_{i-n} \end{Bmatrix} \tag{28}$$

where

$$\mathbf{M}^i_{11} = \mathbf{P}_i(\mathbf{F}_0 + \mathbf{G}_{11}\mathbf{B}_i + \mathbf{G}_{12}\mathbf{B}_{i+1}) \tag{29}$$

$$\mathbf{M}^i_{1n} = -\mathbf{P}_i(\mathbf{G}_{12}\mathbf{B}_i + \mathbf{G}_{13}\mathbf{B}_{i+1}) \tag{30}$$

$$\mathbf{M}^i_{1,n+1} = -\mathbf{P}_i(\mathbf{G}_{11}\mathbf{B}_i + \mathbf{G}_{12}\mathbf{B}_{i+1}) \tag{31}$$

The state transition matrix $\boldsymbol{\psi}$ for the dynamic system over one period T is written as

$$\boldsymbol{\psi} = \mathbf{M}_n\mathbf{M}_{n-1}\cdots\mathbf{M}_1 \tag{32}$$

where

$$\mathbf{M}_i = \begin{bmatrix} \mathbf{M}^i_{11} & 0 & \cdots & 0 & \mathbf{M}^i_{1n} & \mathbf{M}^i_{1,n+1} \\ \mathbf{I} & 0 & \cdots & 0 & 0 & 0 \\ 0 & \mathbf{I} & \cdots & 0 & 0 & 0 \\ \vdots & \vdots & \vdots & \vdots & \vdots & \vdots \\ 0 & 0 & 0 & 0 & \mathbf{I} & 0 \end{bmatrix}, \quad (i = 1, 2, \cdots, n) \tag{33}$$

Then, the stability of the system can be determined according to Floquet theory, the decision criterion is as follows:

$$\max(|\lambda(\boldsymbol{\psi})|) \begin{cases} < 1 & \text{stable} \\ = 1 & \text{critical stable} \\ > 1 & \text{unstable} \end{cases} \tag{34}$$

3.1.2 Second-order shifted Legendre polynomial approximation method

In the second-order shifted Legendre polynomial approximation method (2ndSLPAM), $L_{T,0}(s)$, $L_{T,1}(s)$, and $L_{T,2}(s)$ are adopted to approximate the state term $\mathbf{x}(s)$. Three nodes t_{i-1},

t_i, and t_{i+1} and their nodal values $\mathbf{x}_{i-1}$, $\mathbf{x}_i$, and $\mathbf{x}_{i+1}$ are utilized in the calculation process.

According to Eq. (9), and with the substitutions $t_{i-1} = -\Delta t$, $t_i = 0$, $t_{i+1} = \Delta t$, $L_{T,0}(s)$, $L_{T,1}(s)$, and $L_{T,2}(s)$ can be obtained as follows:

$$L_{T,0}(s) = 1 \tag{35}$$

$$L_{T,1}(s) = \frac{2s-(t_{i-1}+t_{i+1})}{t_{i+1}-t_{i-1}} = \frac{s}{\Delta t} \tag{36}$$

$$L_{T,2}(s) = \frac{3}{2}\cdot\left[\frac{2s-(t_{i-1}+t_{i+1})}{t_{i+1}-t_{i-1}}\right]^2 - \frac{1}{2} = \frac{3s^2}{2(\Delta t)^2} - \frac{1}{2} \tag{37}$$

The coefficients $\mathbf{a}_0$, $\mathbf{a}_1$, and $\mathbf{a}_2$ for $L_{T,0}(s)$, $L_{T,1}(s)$, and $L_{T,2}(s)$, respectively, are derived from Eq. (11) as

$$\mathbf{a}_0 = \frac{\mathbf{x}_{i-1}+\mathbf{x}_i+\mathbf{x}_{i+1}}{3},\quad \mathbf{a}_1 = \frac{-\mathbf{x}_{i-1}+\mathbf{x}_{i+1}}{2},\quad \mathbf{a}_2 = \frac{4}{9}\left(\mathbf{x}_{i-1} - \frac{1}{2}\mathbf{x}_i + \mathbf{x}_{i+1}\right) \tag{38}$$

Combining Eqs. (10), (35), (36), (37), and (38), the state term $\mathbf{x}(s)$ can be expressed as

$$\mathbf{x}(s) = \left[\frac{1}{9} - \frac{s}{2\cdot\Delta t} + \frac{2s^2}{3(\Delta t)^2}\right]\cdot\mathbf{x}_{i-1} + \left[\frac{4}{9} - \frac{s^2}{3(\Delta t)^2}\right]\cdot\mathbf{x}_i + \left[\frac{1}{9} + \frac{s}{2\cdot\Delta t} + \frac{2s^2}{3(\Delta t)^2}\right]\cdot\mathbf{x}_{i+1} \tag{39}$$

The delayed term $\mathbf{x}(s\text{-}\tau)$ and periodic-coefficient matrix $\mathbf{B}(s)$ are still approximated by the first-order shifted orthogonal polynomials with Eqs. (16) and (17), respectively.

Equations (16), (17), and (39) are inserted into (8) to become

$$\mathbf{x}_{i+1} = \mathbf{P}_i\begin{bmatrix}(\mathbf{G}_{21}\mathbf{B}_i + \mathbf{G}_{22}\mathbf{B}_{i+1})\mathbf{x}_{i\text{-}1} + (\mathbf{F}_0 + \mathbf{G}_{23}\mathbf{B}_i + \mathbf{G}_{24}\mathbf{B}_{i+1})\mathbf{x}_i \\ \text{-}(\mathbf{G}_{11}\mathbf{B}_i + \mathbf{G}_{12}\mathbf{B}_{i+1})\mathbf{x}_{i\text{-}n}\text{-}(\mathbf{G}_{12}\mathbf{B}_i + \mathbf{G}_{13}\mathbf{B}_{i+1})\mathbf{x}_{i+1\text{-}n}\end{bmatrix} \tag{40}$$

where

$$\mathbf{G}_{21} = \frac{1}{9}\cdot\mathbf{F}1 - \frac{11}{18\Delta t}\cdot\mathbf{F}2 + \frac{7}{6(\Delta t)^2}\cdot\mathbf{F}3 - \frac{2}{3(\Delta t)^3}\cdot\mathbf{F}4 \tag{41}$$

$$\mathbf{G}_{22} = \frac{1}{9\Delta t}\cdot\mathbf{F}2 - \frac{1}{2(\Delta t)^2}\cdot\mathbf{F}3 + \frac{2}{3(\Delta t)^3}\cdot\mathbf{F}4 \tag{42}$$

$$\mathbf{G}_{23} = \frac{4}{9}\cdot\mathbf{F}1 - \frac{4}{9\Delta t}\cdot\mathbf{F}2 - \frac{1}{3(\Delta t)^2}\cdot\mathbf{F}3 + \frac{1}{3(\Delta t)^3}\cdot\mathbf{F}4 \tag{43}$$

$$\mathbf{G}_{24} = \frac{4}{9\Delta t}\cdot\mathbf{F}2 - \frac{1}{3(\Delta t)^3}\cdot\mathbf{F}4 \tag{44}$$

$$\mathbf{G}_{25} = \frac{1}{9}\,\mathbf{F}1 - \frac{7}{18\Delta t}\cdot\mathbf{F}2 + \frac{1}{6(\Delta t)^2}\cdot\mathbf{F}3 - \frac{2}{3(\Delta t)^3}\cdot\mathbf{F}4 \tag{45}$$

$$\mathbf{G}_{26} = \frac{1}{9\Delta t}\cdot\mathbf{F}2 + \frac{1}{2(\Delta t)^2}\cdot\mathbf{F}3 + \frac{2}{3(\Delta t)^3}\cdot\mathbf{F}4 \tag{46}$$

$$\mathbf{P}_i = [\mathbf{I} - \mathbf{G}_{25}\mathbf{B}_i - \mathbf{G}_{26}\mathbf{B}_{i+1}]^{-1} \tag{47}$$

If $\mathbf{P}_i$ is a nonsingular matrix, the local discrete mapping can be expressed as matrix form according to Eq. (40)

$$\begin{Bmatrix}\mathbf{x}_{i+1}\\ \mathbf{x}_i\\ \mathbf{x}_{i-1}\\ \vdots\\ \mathbf{x}_{i+1-n}\end{Bmatrix} = \begin{bmatrix}\mathbf{M}_{11}^i & \mathbf{M}_{12}^i & \cdots & 0 & \mathbf{M}_{1n}^i & \mathbf{M}_{1,n+1}^i\\ \mathbf{I} & 0 & \cdots & 0 & 0 & 0\\ 0 & \mathbf{I} & \cdots & 0 & 0 & 0\\ \vdots & \vdots & \vdots & \vdots & \vdots & \vdots\\ 0 & 0 & 0 & 0 & \mathbf{I} & 0\end{bmatrix}\begin{Bmatrix}\mathbf{x}_i\\ \mathbf{x}_{i-1}\\ \mathbf{x}_{i-2}\\ \vdots\\ \mathbf{x}_{i-n}\end{Bmatrix} \tag{48}$$

where

$$\mathbf{M}_{11}^i = \mathbf{P}_i(\mathbf{F}_0 + \mathbf{G}_{23}\mathbf{B}_i + \mathbf{G}_{24}\mathbf{B}_{i+1}) \tag{49}$$

$$\mathbf{M}_{12}^i = \mathbf{P}_i(\mathbf{G}_{21}\mathbf{B}_i + \mathbf{G}_{22}\mathbf{B}_{i+1}) \tag{50}$$

$$\mathbf{M}_{1n}^i = -\mathbf{P}_i(\mathbf{G}_{12}\mathbf{B}_i + \mathbf{G}_{13}\mathbf{B}_{i+1}) \tag{51}$$

$$\mathbf{M}_{1,n+1}^i = -\mathbf{P}_i(\mathbf{G}_{11}\mathbf{B}_i + \mathbf{G}_{12}\mathbf{B}_{i+1}) \tag{52}$$

The state transition matrix $\boldsymbol{\psi}$ for the system over one period T is written as

$$\boldsymbol{\psi} = \mathbf{M}_n\mathbf{M}_{n-1}\cdots\mathbf{M}_1 \tag{53}$$

where

$$\mathbf{M}_i = \begin{bmatrix}\mathbf{M}_{11}^i & \mathbf{M}_{12}^i & \cdots & 0 & \mathbf{M}_{1n}^i & \mathbf{M}_{1,n+1}^i\\ \mathbf{I} & 0 & \cdots & 0 & 0 & 0\\ 0 & \mathbf{I} & \cdots & 0 & 0 & 0\\ \vdots & \vdots & \vdots & \vdots & \vdots & \vdots\\ 0 & 0 & 0 & 0 & \mathbf{I} & 0\end{bmatrix},\quad (i = 1, 2, \cdots, n) \tag{54}$$

Then, the stability of milling system can be determined according to Floquet theory, the decision criterion is the same as Eq. (34).

3.1.3 Hyper-second-order shifted Legendre polynomial approximation method

The hyper-second (qth, $q > 2$)-order shifted Legendre polynomial approximation methods ($q$thSLPAM) can also be used to analyze the milling stability on the basis of DIS. In the $q$thSLPAM ($q > 2$), $L_{T,0}(s)$, $L_{T,1}(s)$, $\cdots$, and $L_{T,q}(s)$ are employed to approximate the state term $\mathbf{x}(s)$. The nodes t_{i-q+1}, t_{i-q}, $\cdots$, t_i, and t_{i+1} and their nodal values $\mathbf{x}_{i-q+1}$, $\mathbf{x}_{i-q}$, $\cdots$, $\mathbf{x}_i$, and $\mathbf{x}_{i+1}$ are utilized in the calculation process. The delayed term $\mathbf{x}(s\text{-}\tau)$ and periodic-coefficient matrix $\mathbf{B}(s)$ are still approximated by the first-order shifted Legendre polynomials with Eqs. (16) and (17), respectively.

The higher-order shifted Legendre polynomial approximation methods take more computational time to obtain the stability lobe diagrams, because the number of the '**G**' matrices increase with the increase of the order of approximation methods. Combining with the $q$thSLPAM ($q > 2$) and

Floquet theory, the stability lobe diagrams of milling operations can be obtained. In order to avoid spending duplicate efforts on the similar calculation process, the detailed derivation process of *q*thSLPAM will not be given here. We can refer to the derivation process of the 1stSLPAM and 2ndSLPAM to get an in-depth understanding of *q*thSLPAM.

3.2 Milling stability analysis based on Chebyshev polynomials

Chebyshev polynomials are a set of orthogonal polynomials sequence defined on the interval [−1, 1]. Like the Legendre polynomial approximation methods for milling stability analysis, the Chebyshev polynomials are also applicable for predicting the stability in milling. This section presents the Chebyshev polynomial-based methods for milling stability analysis.

Let $T_l(z)$ and $z \in [-1, 1]$ be the standard Chebyshev polynomial of degree l. The shifted Chebyshev polynomials $T_{T,l}(s)$, $s \in [a, b]$ are defined as

$$T_{T,l}(s) = T_l\left[\frac{2s-(a+b)}{b-a}\right], \quad l = 0, 1, 2, \cdots. \tag{55}$$

In particular,

$$T_{T,0}(s) = 1$$

$$T_{T,1}(s) = \frac{2s-(a+b)}{b-a}$$

$$T_{T,2}(s) = 2\cdot\left[\frac{2s-(a+b)}{b-a}\right]^2 - 1$$

In Eq. (8), the state term **x**(s) can be expressed by using the shifted Chebyshev polynomials as

$$\mathbf{x}(s) = \sum_{k=0}^{l} \mathbf{b}_k \cdot T_{T,k}(s), \quad k \in [0, l] \tag{56}$$

where the coefficient $\mathbf{b}_k$ can be calculated as

$$\mathbf{b}_k = \frac{(\mathbf{x}, T_{T,k})}{(T_{T,k}, T_{T,k})} = \frac{\sum w_j \mathbf{x}_j T_{T,k}(s_j)}{\sum w_j T_{T,k}^2(s_j)} \tag{57}$$

where $\mathbf{x}_j$ is the nodal value of the node s_j, and the weight value $w_j \equiv 1$.

3.2.1 First-order shifted Chebyshev polynomial approximation method

In the first-order Chebyshev polynomial approximation method (1stSCPAM), $T_{T,0}(s)$ and $T_{T,1}(s)$ are adopted to approximate the state term **x**(s). Two nodes t_i and t_{i+1} and their nodal values $\mathbf{x}_i$ and $\mathbf{x}_{i+1}$ are employed for calculation.

Since $T_{T,0}(s)$ and $T_{T,1}(s)$ have the same expressions with those of $L_{T,0}(s)$ and $L_{T,1}(s)$, respectively, the state term **x**(*s*), delayed term **x**(*s*-*τ*) and periodic-coefficient matrix **B**(*s*) obtained by 1stSCPAM are the same with that obtained by 1stSLPAM. Consequently, the detailed calculation process and milling stability lobe diagram calculated by the 1stSCPAM are consistent with those of the 1stSLPAM. Therefore, the derivation process of the milling stability analysis based on 1stSCPAM will not be detailed here. We can refer to the calculation process of 1stSLPAM.

3.2.2 Second-order shifted Chebyshev polynomial approximation method

In the second-order shifted Chebyshev polynomial approximation method, $T_{T,0}(s)$, $T_{T,1}(s)$, and $T_{T,2}(s)$ are adopted to approximate the state term **x**(s). Three nodes t_{i-1}, t_i, and t_{i+1} and their nodal values $\mathbf{x}_{i-1}$, $\mathbf{x}_i$, and $\mathbf{x}_{i+1}$ are utilized for calculation.

According to Eqs. (55)–(57), and with the substitutions $t_{i-1} = -\Delta t$, $t_i = 0$, $t_{i+1} = \Delta t$, the state term **x**(*s*) approximated by the $T_{T,0}(s)$, $T_{T,1}(s)$, and $T_{T,2}(s)$ can be obtained as follows:

$$\mathbf{x}(s) = \left[-\frac{s}{2\cdot\Delta t} + \frac{2s^2}{3(\Delta t)^2}\right]\cdot\mathbf{x}_{i-1} + \left[\frac{2}{3} - \frac{2s^2}{3(\Delta t)^2}\right]\cdot\mathbf{x}_i + \left[\frac{s}{2\cdot\Delta t} + \frac{2s^2}{3(\Delta t)^2}\right]\cdot\mathbf{x}_{i+1} \tag{58}$$

The delayed term **x**(*s*-*τ*) and periodic-coefficient matrix **B**(*s*) are approximated by the first-order shifted Chebyshev polynomials with Eqs. (16) and (17).

Equations (16), (17), and (58) are inserted into (8) to become

$$\mathbf{x}_{i+1} = \mathbf{R}_i\begin{bmatrix}(\mathbf{H}_{21}\mathbf{B}_i + \mathbf{H}_{22}\mathbf{B}_{i+1})\mathbf{x}_{i-1} + (\mathbf{F}_0 + \mathbf{H}_{23}\mathbf{B}_i + \mathbf{H}_{24}\mathbf{B}_{i+1})\mathbf{x}_i \\ -(\mathbf{G}_{11}\mathbf{B}_i + \mathbf{G}_{12}\mathbf{B}_{i+1})\mathbf{x}_{i-n} - (\mathbf{G}_{12}\mathbf{B}_i + \mathbf{G}_{13}\mathbf{B}_{i+1})\mathbf{x}_{i+1-n}\end{bmatrix} \tag{59}$$

where

$$\mathbf{H}_{21} = -\frac{1}{2\Delta t}\cdot\mathbf{F}2 + \frac{7}{6(\Delta t)^2}\cdot\mathbf{F}3 - \frac{2}{3(\Delta t)^3}\cdot\mathbf{F}4 \tag{60}$$

$$\mathbf{H}_{22} = -\frac{1}{2\Delta t}\cdot\mathbf{F}3 + \frac{2}{3(\Delta t)^3}\cdot\mathbf{F}4 \tag{61}$$

$$\mathbf{H}_{23} = \frac{2}{3}\cdot\mathbf{F}1 - \frac{2}{3\Delta t}\cdot\mathbf{F}2 - \frac{2}{3(\Delta t)^2}\cdot\mathbf{F}3 + \frac{2}{3(\Delta t)^3}\cdot\mathbf{F}4 \tag{62}$$

$$\mathbf{H}_{24} = \frac{2}{3(\Delta t)^2}\cdot\mathbf{F}3 - \frac{2}{3(\Delta t)^3}\cdot\mathbf{F}4 \tag{63}$$

$$\mathbf{H}_{25} = \frac{1}{2\Delta t}\cdot\mathbf{F}2 + \frac{1}{6(\Delta t)^2}\cdot\mathbf{F}3 - \frac{2}{3(\Delta t)^3}\cdot\mathbf{F}4 \tag{64}$$

$$\mathbf{H}_{26} = \frac{1}{2(\Delta t)^2}\cdot\mathbf{F}3 + \frac{2}{3(\Delta t)^3}\cdot\mathbf{F}4 \tag{65}$$

$$\mathbf{R}_i = \left[\mathbf{I} - \mathbf{H}_{25}\mathbf{B}_i - \mathbf{H}_{26}\mathbf{B}_{i+1}\right]^{-1} \tag{66}$$

If $\mathbf{R}_i$ is a nonsingular matrix, the local discrete mapping can be expressed as matrix form according to Eq. (59)

$$\begin{Bmatrix} \mathbf{x}_{i+1} \\ \mathbf{x}_i \\ \mathbf{x}_{i-1} \\ \vdots \\ \mathbf{x}_{i+1-n} \end{Bmatrix} = \begin{bmatrix} \mathbf{M}_{11}^i & \mathbf{M}_{12}^i & \cdots & 0 & \mathbf{M}_{1n}^i & \mathbf{M}_{1,n+1}^i \\ \mathbf{I} & 0 & \cdots & 0 & 0 & 0 \\ 0 & \mathbf{I} & \cdots & 0 & 0 & 0 \\ \vdots & \vdots & \vdots & \vdots & \vdots & \vdots \\ 0 & 0 & 0 & 0 & \mathbf{I} & 0 \end{bmatrix} \begin{Bmatrix} \mathbf{x}_i \\ \mathbf{x}_{i-1} \\ \mathbf{x}_{i-2} \\ \vdots \\ \mathbf{x}_{i-n} \end{Bmatrix} \tag{67}$$

where

$$\mathbf{M}_{11}^i = \mathbf{R}_i(\mathbf{F}_0 + \mathbf{H}_{23}\mathbf{B}_i + \mathbf{H}_{24}\mathbf{B}_{i+1}) \tag{68}$$

$$\mathbf{M}_{12}^i = \mathbf{R}_i(\mathbf{H}_{21}\mathbf{B}_i + \mathbf{H}_{22}\mathbf{B}_{i+1}) \tag{69}$$

$$\mathbf{M}_{1n}^i = -\mathbf{R}_i(\mathbf{G}_{12}\mathbf{B}_i + \mathbf{G}_{13}\mathbf{B}_{i+1}) \tag{70}$$

$$\mathbf{M}_{1,n+1}^i = -\mathbf{R}_i(\mathbf{G}_{11}\mathbf{B}_i + \mathbf{G}_{12}\mathbf{B}_{i+1}) \tag{71}$$

The state transition matrix $\boldsymbol{\psi}$ for the system over one period T is written as

$$\boldsymbol{\psi} = \mathbf{M}_n\mathbf{M}_{n-1}\cdots\mathbf{M}_1 \tag{72}$$

where

$$\mathbf{M}_i = \begin{bmatrix} \mathbf{M}_{11}^i & \mathbf{M}_{12}^i & \cdots & 0 & \mathbf{M}_{1n}^i & \mathbf{M}_{1,n+1}^i \\ \mathbf{I} & 0 & \cdots & 0 & 0 & 0 \\ 0 & \mathbf{I} & \cdots & 0 & 0 & 0 \\ \vdots & \vdots & \vdots & \vdots & \vdots & \vdots \\ 0 & 0 & 0 & 0 & \mathbf{I} & 0 \end{bmatrix} \tag{73}$$

Then, the stability of milling system can be determined according to Floquet theory; the decision criterion is the same as Eq. (34).

3.2.3 Hyper-second-order shifted Chebyshev polynomial approximation method

The hyper-second (qth, q >2)-order shifted Chebyshev polynomial approximation methods ($q$thSCPAM) can also be used to analyze the milling stability on the basis of DIS. In the $q$thSCPAM (q > 2), $T_{T,0}(s)$, $T_{T,1}(s)$, ⋯, and $T_{T,q}(s)$ are employed to approximate the state term $\mathbf{x}(s)$. The nodes t_{i-q+1}, t_{i-q}, ⋯, t_i, and t_{i+1} and their nodal values $\mathbf{x}_{i-q+1}$, $\mathbf{x}_{i-q}$, ⋯, $\mathbf{x}_i$, and $\mathbf{x}_{i+1}$ are utilized for calculation. The delayed term $\mathbf{x}(s-\tau)$ and periodic-coefficient matrix $\mathbf{B}(s)$ are still approximated by the first-order shifted Chebyshev polynomials with Eqs. (16) and (17), respectively.

Combining the $q$thSCPAM (q > 2) and Floquet theory, the stability lobe diagram of milling operations can be obtained. The detailed derivation process for $q$thSCPAM will not be given here. We can refer to the calculation process of 1stSCPAM and 2ndSCPAM to gain a better understanding of the $q$thSCPAM.

3.3 Stability lobe diagrams

To demonstrate the applicability of the Legendre and Chebyshev polynomial approximation-based methods in milling, the single DOF and two DOF milling models are taken as the examples for analysis. The 1stSDM is an experimentally validated and widely used method for milling stability prediction. Therefore, this paper takes the 1stSDM as benchmark for the comparison of prediction results. The stability lobe diagrams obtained by 1stSLPAM, 2ndSLPAM, 3rdSLPAM, 1stSCPAM, 2ndSCPAM, and 3rdSCPAM are compared with that obtained by benchmark 1stSDM.

3.3.1 Single DOF milling model

The stability lobe diagrams are generated over 100 × 100 sized grid of parameters of spindle speed Ω and axial depth of cut a_p. The radial depth of cut ratio a_e/D is chosen as 0.1, 0.5, and 1. The machining parameters are chosen as the same as literature [13] to generate stability lobe diagrams. The parameters are as follows: the number of tooth N = 2, the natural frequency f_n = 922 Hz, the relative damping is ζ = 0.011, the modal mass is m = 0.03993 kg, the cutting force coefficients are $K_t = 6 \times 10^8$ N/m^2, and $K_n = 2 \times 10^8$ N/m^2, down milling. The program is conducted using Matlab 2010a software on a computer with Intel (R) Core (TM) i3-2120 and 2 GB memory. The stability lobe diagrams calculated by 1stSDM with n = 100 are taken as the ideal results. Stability lobe diagrams for single DOF milling model obtained by 1stSDM, 1stSLPAM, 2ndSLPAM, 3rdSLPAM, 1stSCPAM, 2ndSCPAM, and 3rdSCPAM are shown in Table 1.

In Table 1, the red line curves represent the ideal stability lobe diagrams; the blue line curves represent the actual stability lobe diagrams. The prediction results of the 1stSLPAM and 1stSCPAM are the same, so the

Table 1 Stability lobe diagrams for single DOF milling model obtained by 1stSDM, 1stSLPAM, 2ndSLPAM, 3rdSLPAM, 1stSCPAM, 2ndSCPAM, and 3rdSCPAM

Methods	n=30, a_e/D=0.1	n=40, a_e/D=0.5	n=50, a_e/D=1
1stSDM	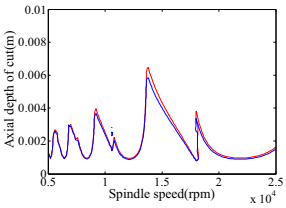	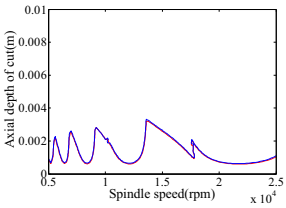	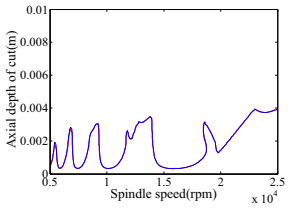
1stSLPAM/ 1stSCPAM	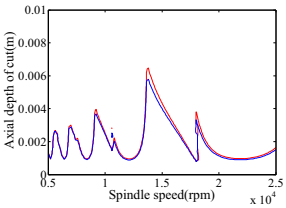	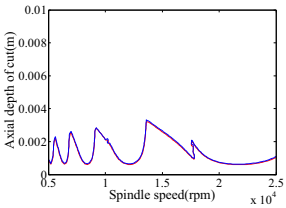	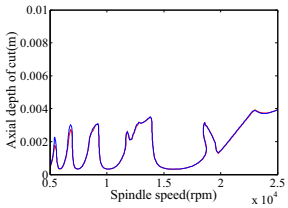
2ndSLPAM	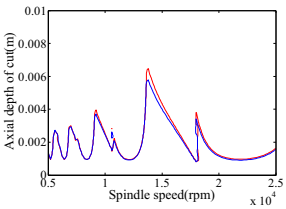	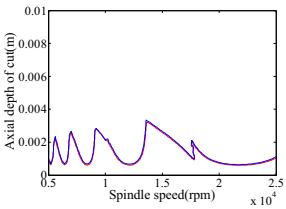	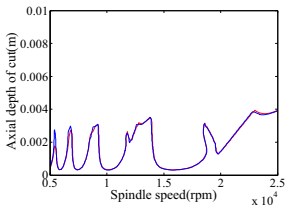
3rdSLPAM	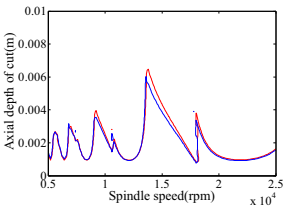	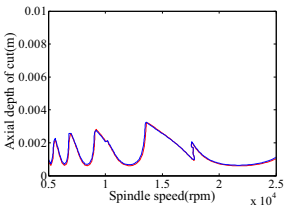	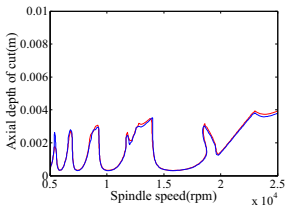
2ndSCPAM	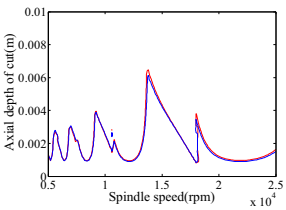	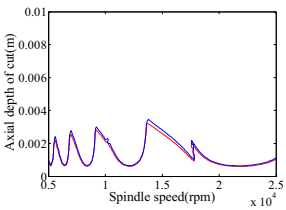	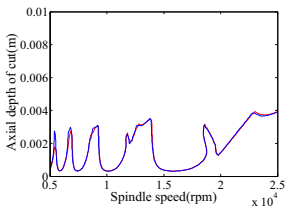
3rdSCPAM	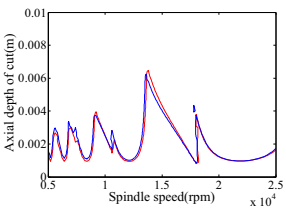	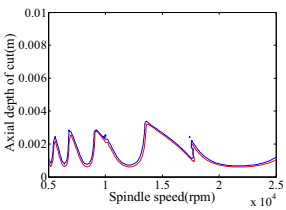	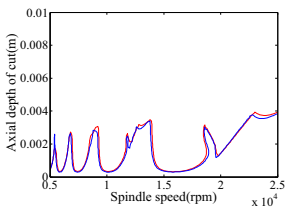

stability lobe diagrams of these two methods are listed in one line. As shown in Table 1, for different radial depth of cut ratios a_e/D, the stability lobe diagrams obtained by 1stSLPAM, 2ndSLPAM, 3rdSLPAM, 1stSCPAM,

2ndSCPAM, and 3rdSCPAM are consistent with the ideal stability lobe diagrams, which indicates that the Legendre and Chebyshev polynomial approximation-based methods are reliable and applicable for milling stability prediction. In order to make the predicted results more applicable to actual situation, the two DOF milling model considering the flexibility of the milling tool in both X and Y direction is also analyzed.

3.3.2 Two DOF milling model

The governing equation of system motion of a two DOF milling model can be expressed in the following state space form:

$$\dot{\mathbf{u}}(t) = \mathbf{A}\mathbf{u}(t) + \mathbf{B}(t)\mathbf{u}(t) - \mathbf{B}(t)\mathbf{u}(t-\tau) \tag{74}$$

where

$$\mathbf{A} = \begin{bmatrix} 0 & 0 & 1 & 0 \\ 0 & 0 & 0 & 1 \\ -\omega_n^2 & 0 & -2\zeta\omega_n & 0 \\ 0 & -\omega_n^2 & 0 & -2\zeta\omega_n \end{bmatrix}, \mathbf{B}(t) = \begin{bmatrix} 0 & 0 & 0 & 0 \\ 0 & 0 & 0 & 0 \\ \frac{-a_p h_{xx}(t)}{m} & \frac{-a_p h_{xy}(t)}{m} & 0 & 0 \\ \frac{-a_p h_{yx}(t)}{m} & \frac{-a_p h_{yy}(t)}{m} & 0 & 0 \end{bmatrix}$$

$$\mathbf{u}(t) = \begin{bmatrix} x(t) \\ y(t) \\ \dot{x}(t)\dot{y}(t) \end{bmatrix}$$

In matrix $\mathbf{B}(t)$, four projections of the specific cutting force coefficient, i.e., h_{xx}, h_{xy}, h_{yx}, h_{yy}, are expressed as

$$h_{xx}(t) = \sum_{j=1}^{N} g\left[\varphi_j(t)\right] \sin\left(\varphi_j(t)\right) \left[K_t \cos\left(\varphi_j(t)\right) + K_n \sin\left(\varphi_j(t)\right)\right] \tag{75}$$

$$h_{xy}(t) = \sum_{j=1}^{N} g\left[\varphi_j(t)\right] \cos\left(\varphi_j(t)\right) \left[K_t \cos\left(\varphi_j(t)\right) + K_n \sin\left(\varphi_j(t)\right)\right] \tag{76}$$

$$h_{yx}(t) = \sum_{j=1}^{N} g\left[\varphi_j(t)\right] \sin\left(\varphi_j(t)\right) \left[-K_t \sin\left(\varphi_j(t)\right) + K_n \cos\left(\varphi_j(t)\right)\right] \tag{77}$$

$$h_{yy}(t) = \sum_{j=1}^{N} g\left[\varphi_j(t)\right] \cos\left(\varphi_j(t)\right) \left[-K_t \sin\left(\varphi_j(t)\right) + K_n \cos\left(\varphi_j(t)\right)\right] \tag{78}$$

On the basis of DIS, the stability lobe diagrams for two DOF milling model can also be obtained by using Legendre and Chebyshev polynomial approximation-based methods. The parameters used for two DOF milling model are the same with those used in single DOF milling model and assumed to be equal in X and Y directions. The stability lobe diagrams are calculated over 100 × 100 sized grid of spindle speed Ω and the axial depth of cut a_p. The stability lobe diagrams for two DOF milling model calculated by 1stSDM with n = 100 are taken as the ideal results. The stability lobe diagrams for two DOF milling model obtained by 1stSDM, 1stSLPAM, 2ndSLPAM, 3rdSLPAM, 1stSCPAM, 2ndSCPAM, and 3rdSCPAM are shown in Table 2.

As shown in Table 2, the stability lobe diagrams for two DOF milling model obtained by 1stSLPAM, 2ndSLPAM, 3rdSLPAM, 1stSCPAM, 2ndSCPAM, and 3rdSCPAM are consistent with the ideal stability lobe diagrams. The comparison results of the stability lobe diagrams indicate that the Legendre and Chebyshev polynomial approximation-based methods are also applicable to the two DOF milling model. Additionally, as the parameter n increase, the stability lobe diagrams are closer to the ideal ones.

3.4 The rate of convergence analysis

The rate of convergence respects the local errors between the absolute value of the maximal critical eigenvalues of the state transition matrix $|\mu(n)|$ and the exact eigenvalue μ_0, where $|\mu(n)|$ is a function of computational parameter n. The exact eigenvalue μ_0 is determined by the 1stSDM with n = 200. To study the rate of convergence of the Legendre and Chebyshev polynomial approximation-based methods, the radial depth of cut ratio a_e/D is set as 1 to avoid intermittent milling, the spindle speed is Ω = 5000 rpm, and the axial depth of cut is chosen as a_p = 0.2 and 0.5 mm, respectively. The rate of convergence of the 1stSLPAM, 2ndSLPAM, 3rdSLPAM, 1stSCPAM, 2ndSCPAM, and 3rdSCPAM is analyzed by comparing with that of the 1stSDM.

The program is conducted using Matlab 2010a software on a computer with Intel (R) Core (TM) i3-2120 and 2 GB memory. The parameters used for the rate of convergence analysis are the same with those used in section 3.3. Figure 2 illustrates the convergences of the eigenvalues with different computational parameters n for different methods.

As shown in Fig.2a, b, the 1stSLPAM and 1stSCPAM have the same rate of convergence because the state transition matrixes $\boldsymbol{\psi}$ obtained by these two methods are the same. The local errors calculated by 1stSLPAM and 1stSCPAM are both greater than that calculated by 1stSDM, which means the rate of convergence of the 1stSDM is higher than that of the 1stSLPAM and 1stSCPAM.

As shown in Fig.2a, b, with regard to the second-order approximation methods, the local errors of 2ndSLPAM cannot reach numerical stability, because when the parameter n approaches to 100 gradually, the local errors calculated by 2ndSLPAM still have an increasing trend, that is, the local errors of 2ndSLPAM do not reach a stable state eventually. The 2ndSCPAM has the numerical stability because the local errors obtained by 2ndSCPAM decrease with the increase of parameter n, and eventually the local approximation errors reach steady state. It is also seen from Fig. 2a, b that the 1stSDM is of higher computation accuracy than that of 2ndSCPAM. According to Fig. 2a, when the parameter n is greater than 41, the computation accuracy of 2ndSLPAM is higher than that of 1stSDM. When the parameter n is equal to 69, the minimum local

Table 2 Stability lobe diagrams for two DOF milling model obtained by 1stSDM, 1stSLPAM, 2ndSLPAM, 3rdSLPAM, 1stSCPAM, 2ndSCPAM, and 3rdSCPAM

Methods	n=30, a_e/D=0.1	n=40, a_e/D=0.5	n=50, a_e/D=1
1stSDM	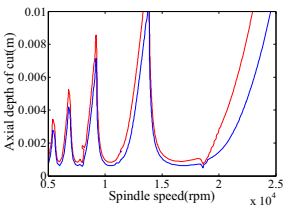	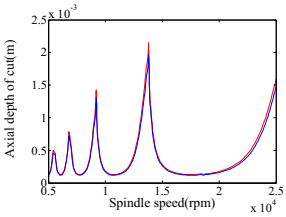	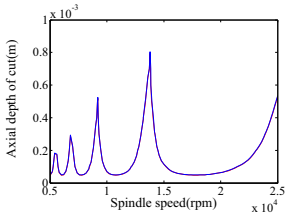
1stSLPAM/ 1stSCPAM	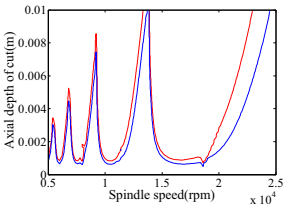	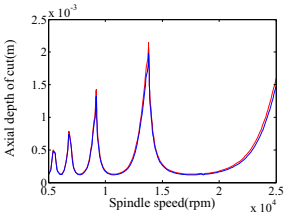	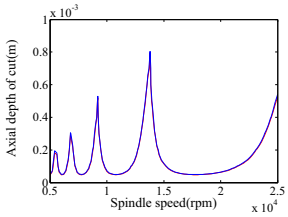
2ndSLPAM	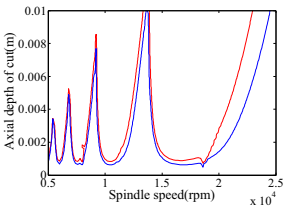	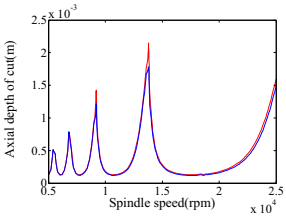	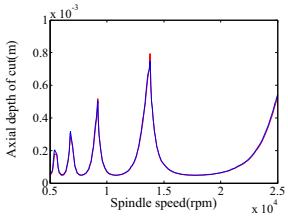
3rdSLPAM	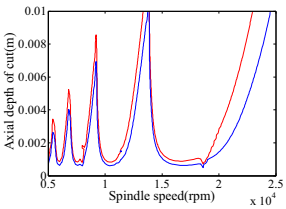	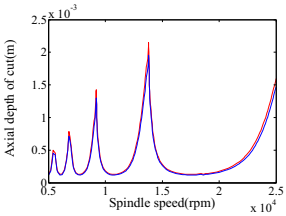	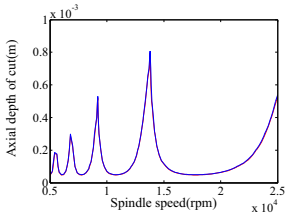
2ndSCPAM	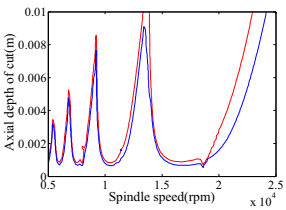	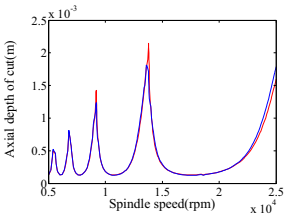	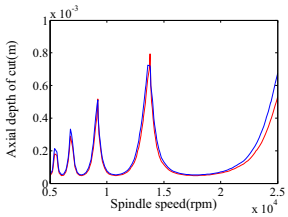
3rdSCPAM	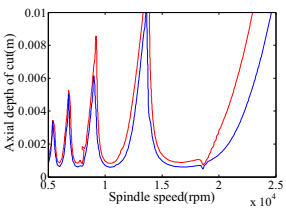	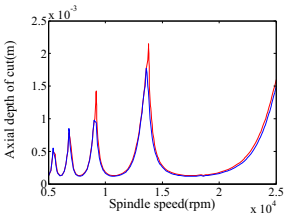	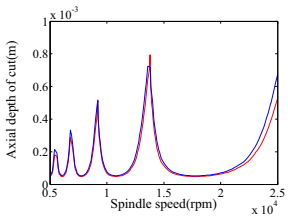

error is obtained, and then the local approximation errors increase with the increase of parameter n.

As for the third-order approximation methods, the rates of convergence of the 3rdSLPAM and 3rdSCPAM are

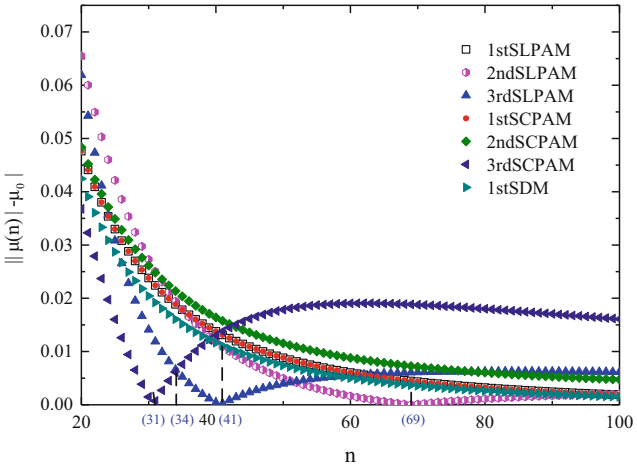

(a) a_p=0.2 mm, $|\mu_0|$=0.81923867 (stable)

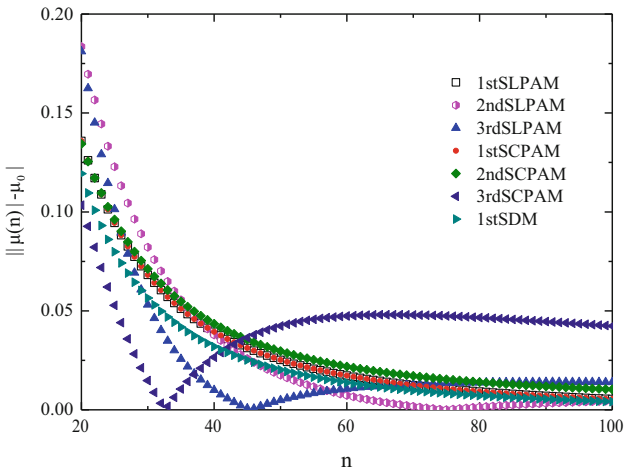

(b) a_p=0.5 mm, $|\mu_0|$= 1.07260456 (unstable)

Fig. 2 The rates of convergence of the 1stSDM, 1stSLPAM, 2ndSLPAM, 3rdSLPAM, 1stSCPAM, 2ndSCPAM, and 3rdSLPAM. **a** *ap* = 0.2 mm, $|\mu 0|$ = 0.81923867 (stable). **b** *ap* = 0.5 mm, $|\mu 0|$ = 1.07260456 (unstable)

sensitive to the parameter *n*. As shown in Fig. 2a, b, the variation trends of the rate of convergence for 3rdSLPAM and 3rdSCPAM vary with the parameter *n*; they do not exhibit the monotonic increasing or decreasing features with respect to *n*. In Fig. 2a, when the parameter *n* is less than 34, the computation accuracy of 3rdSCPAM is superior to other methods; when the parameter *n* is less than 31, the local errors decrease with the decrease of parameter *n*, and the minimum local error is obtained when *n* is equal to 31. Unlike the 3rdSCPAM of which the local approximation errors do not reach a stable state, the local errors calculated by 3rdSLPAM remain stable state at last. As the parameter *n* is close to 100 gradually, the local errors calculated by 3rdSCPAM are much greater than those of 3rdSLPAM. The comparison results of Fig. 2b have the similar trend with Fig. 2a although these two figures reflect two different milling operations (stable and unstable).

In mathematical theory, higher-order approximation methods may lead to more accurate results. However, in this section, the higher-order Legendre and Chebyshev approximation-based methods do not result in more accurate results. In order to predict the milling stability precisely, the methods which have both numerical stability and high rate of convergence are required. With the aim of developing new orthogonal polynomial approximation-based methods to predict milling stability based on DIS, a kind of monic orthogonal polynomial sequence which can be deduced by Gram-Schmidt orthogonalization [21] is employed to approximated the state term $\mathbf{x}(s)$, delayed term $\mathbf{x}(s\text{-}\tau)$, and periodic-coefficient matrix $\mathbf{B}(s)$.

4 Monic orthogonal polynomials for milling stability prediction

In this section, the monic orthogonal polynomials are constructed using Gram-Schmidt orthogonalization. The constructed monic orthogonal polynomials can be used to obtain the state transition matrix $\boldsymbol{\psi}$. Unlike the Legendre and Chebyshev approximation-based methods in which the interval conversion should be performed first, the monic orthogonal polynomial approximation-based methods can be used without interval conversion.

Without loss of generality, on the basis of Gram-Schmidt orthogonalization, the monic orthogonal polynomials can be generated by the following recurrence:

$$\begin{cases} P_0(s) = 1 \\ P_1(s) = s - \alpha_1 \\ P_l(s) = (s-\alpha_l)P_{l-1} - \beta_l P_{l-2}(s) \qquad (l \geq 1) \end{cases} \tag{79}$$

where

$$\alpha_l = \frac{\int_0^T s w P_{l-1}^2(s)ds}{\int_0^T w P_{l-1}^2(s)ds} = \frac{\sum w_j s_j P_{l-1}^2(s_j)}{\sum w_j P_{l-1}^2(s_j)}, \quad \beta_l = \frac{\int_0^T w P_{l-1}^2(s)ds}{\int_0^T w P_{l-2}^2(s)ds} = \frac{\sum w_j P_{l-1}^2(s_j)}{\sum w_j P_{l-2}^2(s_j)} \tag{80}$$

where $w_j \equiv 1$, s_j represents the selected node.

In Eq. (8), the state term $\mathbf{x}(s)$ can be approximated by the monic orthogonal polynomials as

$$\mathbf{x}(s) = \sum_{k=0}^{l} \mathbf{c}_k \cdot P_k(s), \quad k \in [0, l] \tag{81}$$

where the coefficient $\mathbf{c}_k$ can be calculated as

$$\mathbf{c}_k = \frac{(\mathbf{x}, P_k)}{(P_k, P_k)} = \frac{\sum w_j \mathbf{x}_j P_k(s_j)}{\sum w_j P_k^2(s_j)} \tag{82}$$

where $\mathbf{x}_j$ is the nodal value of the node s_j.

4.1 First-order monic orthogonal polynomial approximation method

In the first-order monic orthogonal polynomial approximation method (1stMOPAM), $P_0(s)$ and $P_1(s)$ are employed to approximate the state term $\mathbf{x}(s)$. Two nodes t_i and t_{i+1} and their nodal values $\mathbf{x}_i$ and $\mathbf{x}_{i+1}$ are used in the calculation process.

On the basis of Eq. (80), α_1 can be obtained as

$$\alpha_1 = \frac{\sum_{j=i}^{i+1} w_j s_j P_0^2(s_j)}{\sum_{j=i}^{i+1} w_j P_0^2(s_j)} = \frac{t_i + t_{i+1}}{2}$$

With the substitutions $t_i = 0$ and $t_{i+1} = \Delta t$, α_1 can be rewritten as $\alpha_1 = \frac{\Delta t}{2}$.

According to Eq. (79), $P_0(s)$ and $P_1(s)$ can be represented as

$$P_0(s) = 1, \quad P_1(s) = s - \frac{\Delta t}{2} \tag{83}$$

The state term $\mathbf{x}(s)$ can be expressed as

$$\mathbf{x}(s) = \mathbf{c}_0 P_0(s) + \mathbf{c}_1 P_1(s) = \mathbf{c}_0 \cdot 1 + \mathbf{c}_1 \cdot \left(s - \frac{\Delta t}{2}\right) \tag{84}$$

where coefficients $\mathbf{c}_0$ and $\mathbf{c}_1$ can be obtained according to Eq. (82) as

$$\mathbf{c}_0 = \frac{\sum_{j=i}^{i+1} w_j \mathbf{x}_j P_0(s_j)}{\sum_{j=i}^{i+1} w_j P_0^2(s_j)} = \frac{\mathbf{x}_i + \mathbf{x}_{i+1}}{2}, \quad \mathbf{c}_1 = \frac{\sum_{j=i}^{i+1} w_j \mathbf{x}_j P_1(s_j)}{\sum_{j=i}^{i+1} w_j P_1^2(s_j)} = \frac{\mathbf{x}_{i+1} - \mathbf{x}_i}{\Delta t} \tag{85}$$

Submitting Eq. (85) into Eq. (84) leads to

$$\mathbf{x}(s) = \left(1 - \frac{s}{\Delta t}\right) \cdot \mathbf{x}_i + \frac{s}{\Delta t} \cdot \mathbf{x}_{i+1} \tag{86}$$

Similarly, the delayed term $\mathbf{x}(s\text{-}\tau)$ and periodic-coefficient matrix $\mathbf{B}(s)$ can be represented as

$$\mathbf{x}(s - \tau) = \left(1 - \frac{s}{\Delta t}\right) \cdot \mathbf{x}_{i-n} + \frac{s}{\Delta t} \cdot \mathbf{x}_{i-n+1} \tag{87}$$

$$\mathbf{B}(s) = \left(1 - \frac{s}{\Delta t}\right) \cdot \mathbf{B}_i + \frac{s}{\Delta t} \cdot \mathbf{B}_{i+1} \tag{88}$$

It is obviously found that the state term $\mathbf{x}(s)$, delayed term $\mathbf{x}(s\text{-}\tau)$, and periodic-coefficient matrix $\mathbf{B}(s)$ obtained by 1stMOPAM are the same with those obtained by 1stSLPAM. Consequently, the state transition matrix $\boldsymbol{\psi}$ and the stability lobe diagram obtained by 1stMOPAM are also the same with those obtained by 1stSLPAM. Therefore, the subsequent derivation process of the milling stability analysis using 1stMOPAM will not be detailed here. We can refer to the calculation process of 1stSLPAM.

4.2 Second-order monic orthogonal polynomial approximation method

In the second-order monic orthogonal polynomial approximation method (2ndMOPAM), $P_0(s)$, $P_1(s)$, and $P_2(s)$ are adopted to approximate the state term $\mathbf{x}(s)$. Three nodes t_{i-1}, t_i, and t_{i+1} as well as their nodal values $\mathbf{x}_{i-1}$, $\mathbf{x}_{i+1}$, and $\mathbf{x}_i$ are utilized for calculation.

$P_0(s)$, $P_1(s)$, and $P_2(s)$ satisfy the following three-term recurrence relation:

$$\begin{cases} P_0(s) = 1 \\ P_1(s) = s - \alpha_1 \\ P_2(s) = (s - \alpha_2) P_1(s) - \beta_2 P_1(s) \end{cases} \tag{89}$$

According to Eqs. (80) and (89), and with the substitutions $t_{i-1} = -\Delta t$, $t_i = 0$, $t_{i+1} = \Delta t$, the coefficients α_1, α_2, and β_2 can be obtained as

$$\alpha_1 = \frac{\sum_{j=i-1}^{i+1} w_j s_j P_0^2(s_j)}{\sum_{j=i-1}^{i+1} w_j P_0^2(s_j)} = 0, \quad \alpha_2 = \frac{\sum_{j=i-1}^{i+1} w_j s_j P_1^2(s_j)}{\sum_{j=i-1}^{i+1} w_j P_1^2(s_j)}$$

$$= 0, \quad \beta_2 = \frac{\sum_{j=i-1}^{i+1} w_j P_1^2(s_j)}{\sum_{j=i-1}^{i+1} w_j P_0^2(s_j)} = \frac{2}{3}(\Delta t)^2$$

Then, $P_0(s)$, $P_1(s)$, and $P_2(s)$ can be rewritten as

$$P_0(s) = 1, \quad P_1(s) = s, \quad P_2(s) = s^2 - \frac{2}{3}(\Delta t)^2 \tag{90}$$

The coefficients $\mathbf{c}_0$, $\mathbf{c}_1$, and $\mathbf{c}_2$ for $P_0(s)$, $P_1(s)$, and $P_2(s)$, respectively, are derived from Eq. (82) as

$$\mathbf{c}_0 = \frac{\mathbf{x}_{i-1} + \mathbf{x}_i + \mathbf{x}_{i+1}}{3}, \quad \mathbf{c}_1 = \frac{-\mathbf{x}_{i-1} + \mathbf{x}_{i+1}}{2\Delta t}, \quad \mathbf{c}_2 = \frac{\mathbf{x}_{i-1} - 2\mathbf{x}_i + \mathbf{x}_{i+1}}{2(\Delta t)^2} \tag{91}$$

Combining Eqs. (90) and (91), the state term $\mathbf{x}(s)$ can be expressed as

$$\mathbf{x}(s) = \left(\frac{s^2}{2(\Delta t)^2} - \frac{s}{2\Delta t}\right)\mathbf{x}_{i-1} + \left(1 - \frac{s^2}{(\Delta t)^2}\right)\mathbf{x}_i + \left(\frac{s^2}{2(\Delta t)^2} + \frac{s}{2\Delta t}\right)\mathbf{x}_{i+1} \tag{92}$$

The delayed term $\mathbf{x}(s\text{-}\tau)$ and periodic-coefficient matrix $\mathbf{B}(s)$ are still approximated by the first-order monic orthogonal polynomials with Eqs. (87) and (88), respectively.

Substituting Eqs. (87), (88), and (92) into Eq. (8) results in

$$\mathbf{x}_{i+1} = \mathbf{U}_i \begin{bmatrix} (\mathbf{V}_{21}\mathbf{B}_i + \mathbf{V}_{22}\mathbf{B}_{i+1})\mathbf{x}_{i-1} + (\mathbf{F}_0 + \mathbf{V}_{23}\mathbf{B}_i + \mathbf{V}_{24}\mathbf{B}_{i+1})\mathbf{x}_i \\ -(\mathbf{G}_{11}\mathbf{B}_i + \mathbf{G}_{12}\mathbf{B}_{i+1})\mathbf{x}_{i-m} - (\mathbf{G}_{12}\mathbf{B}_i + \mathbf{G}_{13}\mathbf{B}_{i+1})\mathbf{x}_{i+1-m} \end{bmatrix} \quad (93)$$

where

$$\mathbf{V}_{21} = -\frac{1}{2\Delta t}\cdot\mathbf{F}2 + \frac{1}{(\Delta t)^2}\cdot\mathbf{F}3 - \frac{1}{2(\Delta t)^3}\cdot\mathbf{F}4 \quad (94)$$

$$\mathbf{V}_{22} = -\frac{1}{2(\Delta t)^2}\cdot\mathbf{F}3 + \frac{1}{2(\Delta t)^3}\cdot\mathbf{F}4 \quad (95)$$

$$\mathbf{V}_{23} = \mathbf{F}1 - \frac{1}{\Delta t}\cdot\mathbf{F}2 - \frac{1}{(\Delta t)^2}\cdot\mathbf{F}3 + \frac{1}{(\Delta t)^3}\cdot\mathbf{F}4 \quad (96)$$

$$\mathbf{V}_{24} = \frac{1}{\Delta t}\cdot\mathbf{F}2 - \frac{1}{(\Delta t)^3}\cdot\mathbf{F}4 \quad (97)$$

$$\mathbf{V}_{25} = \frac{1}{2\Delta t}\cdot\mathbf{F}2 - \frac{1}{2(\Delta t)^3}\cdot\mathbf{F}4 \quad (98)$$

$$\mathbf{V}_{26} = \frac{1}{2(\Delta t)^2}\cdot\mathbf{F}3 + \frac{1}{2(\Delta t)^3}\cdot\mathbf{F}4 \quad (99)$$

$$\mathbf{U}_i = [\mathbf{I} - \mathbf{V}_{25}\mathbf{B}_i - \mathbf{V}_{26}\mathbf{B}_{i+1}]^{-1} \quad (100)$$

Table 3 Stability lobe diagrams for single DOF milling model obtained by 1stSDM, 1stMOPAM, 2ndMOPAM, and 3rdMOPAM

Methods	n=30, a_e/D=0.1	n=40, a_e/D=0.5	n=50, a_e/D=1
1stSDM	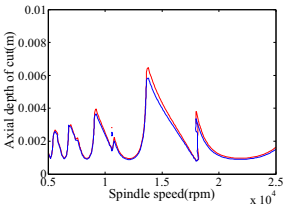 Time=105s	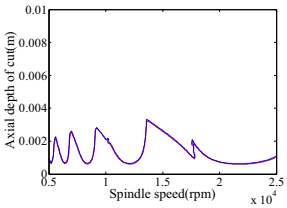 Time=157s	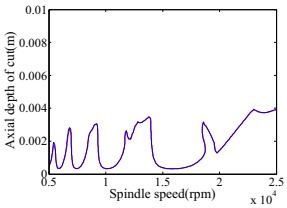 Time=233s
1stMOPAM	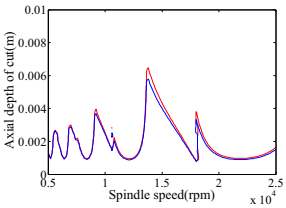 Time=21s	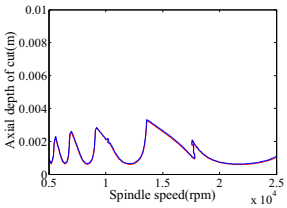 Time=47s	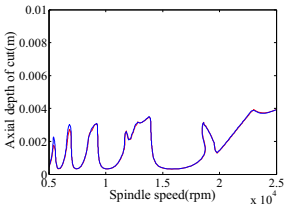 Time=92s
2ndMOPAM	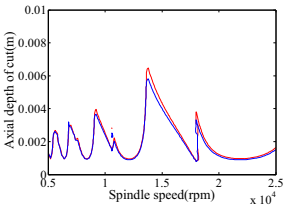 Time=23s	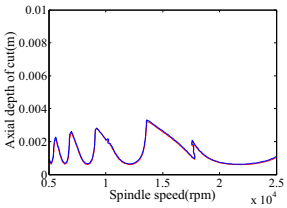 Time=50s	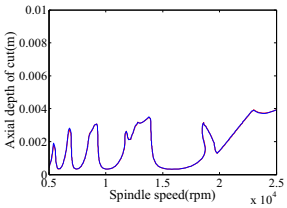 Time=96s
3rdMOPAM	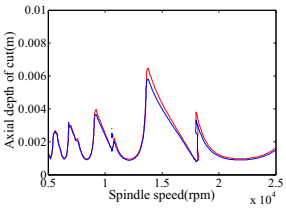 Time=26s	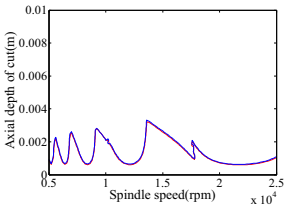 Time=52s	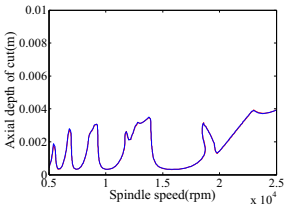 Time=99s

If $\mathbf{U}_i$ is a nonsingular matrix, the local discrete map can be expressed as matrix form according to Eq. (93)

$$\begin{Bmatrix} \mathbf{x}_{i+1} \\ \mathbf{x}_i \\ \mathbf{x}_{i-1} \\ \vdots \\ \mathbf{x}_{i+1-m} \end{Bmatrix} = \begin{bmatrix} \mathbf{M}_{11}^i & \mathbf{M}_{12}^i & \cdots & 0 & \mathbf{M}_{1m}^i & \mathbf{M}_{1,m+1}^i \\ \mathbf{I} & 0 & \cdots & 0 & 0 & 0 \\ 0 & \mathbf{I} & \cdots & 0 & 0 & 0 \\ \vdots & \vdots & \vdots & \vdots & \vdots & \vdots \\ 0 & 0 & 0 & 0 & \mathbf{I} & 0 \end{bmatrix} \begin{Bmatrix} \mathbf{x}_i \\ \mathbf{x}_{i-1} \\ \mathbf{x}_{i-2} \\ \vdots \\ \mathbf{x}_{i-m} \end{Bmatrix} \quad (101)$$

and

$$\mathbf{M}_{12}^i = \mathbf{U}_i(\mathbf{F}_0 + \mathbf{V}_{23}\mathbf{B}_i + \mathbf{V}_{24}\mathbf{B}_{i+1}) \quad (102)$$

$$\mathbf{M}_{12}^i = \mathbf{U}_i(\mathbf{V}_{21}\mathbf{B}_i + \mathbf{V}_{22}\mathbf{B}_{i+1}) \quad (103)$$

$$\mathbf{M}_{1m}^i = -\mathbf{U}_i(\mathbf{G}_{12}\mathbf{B}_i + \mathbf{G}_{13}\mathbf{B}_{i+1}) \quad (104)$$

$$\mathbf{M}_{1,m+1}^i = -\mathbf{U}_i(\mathbf{G}_{11}\mathbf{B}_i + \mathbf{G}_{12}\mathbf{B}_{i+1}) \quad (105)$$

The transition matrix ψ for the system over one period T is written as

$$\psi = \mathbf{M}_m\mathbf{M}_{m-1}\cdots\mathbf{M}_1 \quad (106)$$

and

$$\mathbf{M}_i = \begin{bmatrix} \mathbf{M}_{11}^i & \mathbf{M}_{12}^i & \cdots & 0 & \mathbf{M}_{1m}^i & \mathbf{M}_{1,m+1}^i \\ \mathbf{I} & 0 & \cdots & 0 & 0 & 0 \\ 0 & \mathbf{I} & \cdots & 0 & 0 & 0 \\ \vdots & \vdots & \vdots & \vdots & \vdots & \vdots \\ 0 & 0 & 0 & 0 & \mathbf{I} & 0 \end{bmatrix} \quad (107)$$

Then, the stability of milling system can be determined according to Floquet theory.

4.3 Hyper-second-order monic orthogonal polynomial approximation method

The hyper-second (qth, $q > 2$)-order monic orthogonal polynomial approximation methods ($q$thMOPAM) can also be used to analyze the milling stability on the basis of DIS. In the $q$thMOPAM ($q > 2$), $P_0(s)$, $P_1(s)$, ⋯, and $P_q(s)$ are employed to approximate the state term $\mathbf{x}(s)$. The nodes t_{i-q+1}, t_{i-q}, ⋯, t_i, and t_{i+1} and their nodal values $\mathbf{x}_{i-q+1}$, $\mathbf{x}_{i-q}$, ⋯, $\mathbf{x}_i$, and $\mathbf{x}_{i+1}$ are utilized for calculation. The delayed term $\mathbf{x}(s\text{-}\tau)$ and periodic-coefficient matrix $\mathbf{B}(s)$ are still approximated by the first-order monic orthogonal polynomials with Eqs. (87) and (88), respectively.

The higher order monic orthogonal polynomial approximation methods take more computation time to generate the stability lobe diagram, because the number of the '**V**' matrices increases with the increase of the order of approximation methods. Combining the $q$thMOPAM ($q > 2$) and Floquet theory, the stability lobe diagram of milling operations can be obtained. The detailed derivation process of $q$thMOPAM is not given here. We can refer to the derivation process of 1stMOPAM and 2ndMOPAM to gain an in-depth understanding of $q$thMOPAM.

4.4 Stability lobe diagrams

4.4.1 Single DOF milling model

In order to illustrate the applicability and computational accuracy of the monic orthogonal polynomial approximation-based methods, the stability lobe diagrams calculated by 1stMOPAM, 2ndMOPAM, and 3rdMOPAM are compared with that calculated by benchmark 1stSDM. The parameters used for the monic orthogonal polynomial approximation-based methods are the same with those used in Legendre and Chebyshev approximation-based methods. The stability charts are calculated over 100 × 100 sized grid with the axial depth of cut ranging from 0 to 0.01 m, and the spindle speed ranging from 5×10^3 to 25×10^3 rpm. The stability lobe diagrams calculated by 1stSDM with $n = 100$ are taken as the ideal results. The stability lobe diagrams for single DOF milling model obtained by 1stSDM, 1stMOPAM, 2ndMOPAM, and 3rdMOPAM are shown in Table 3.

It is seen form Table 3 that the stability lobe diagrams obtained by 2ndMOPAM and 3rdMOPAM are closer to the ideal curves than that obtained by 1stSDM. As shown in Table 3, the stability lobe diagrams of 3rdMOPAM with $n = 50$ is highly identical to that of 1stSDM with $n = 100$. Therefore, compared with benchmark 1stSDM, the 3rdMOPAM can generate accurate stability lobe diagrams with a small value of the parameter n. It is also indicated form Table 3 that the monic orthogonal polynomial approximation-based methods take less time than the

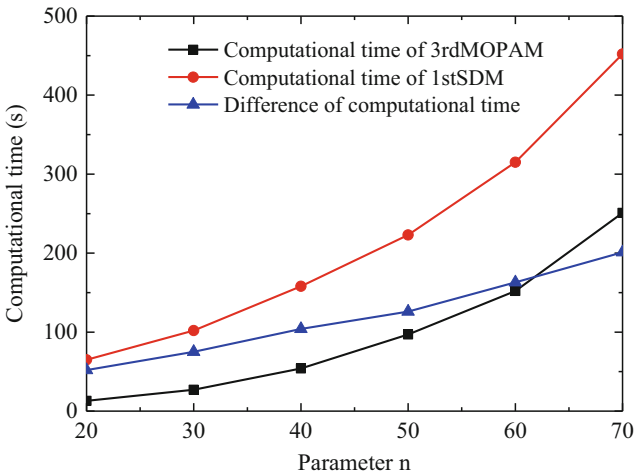

Fig. 3 Comparison of the time-consuming convergence for single DOF milling model of the 1stSDM and the 3rdMOPAM

Table 4 Stability lobe diagrams obtained by 1stSDM, 1stMOPAM, 2ndMOPAM, and 3rdMOPAM for two DOF milling model

Methods	n=30, a_e/D=0.1	n=40, a_e/D=0.5	n=50, a_e/D=1
1stSDM	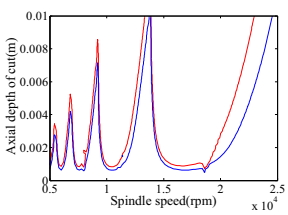	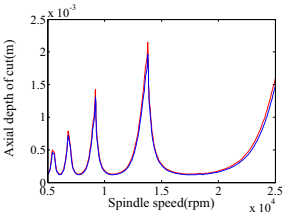	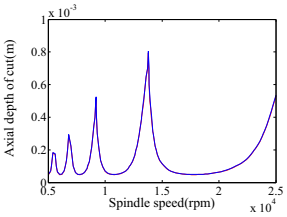
	185s	358s	665s
1stMOPAM	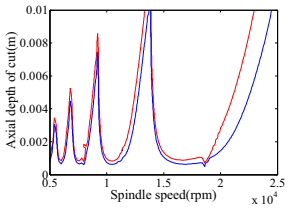	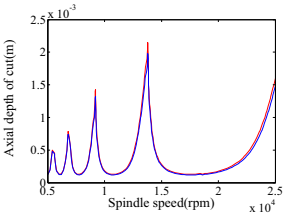	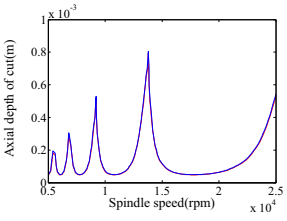
	Time=76s	Time=203s	Time=478s
2ndMOPAM	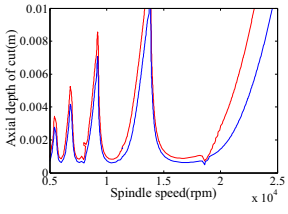	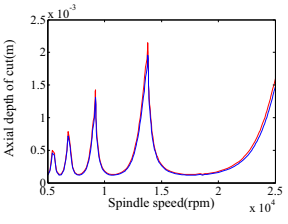	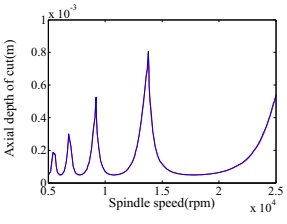
	Time=83s	Time=212s	Time=490s
3rdMOPAM	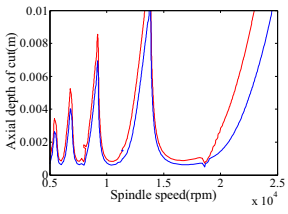	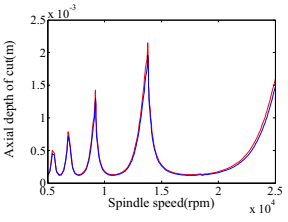	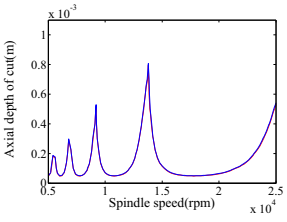
	89s	225s	520s

1stSDM to generate stability lobe diagrams with the same parameter n.

In order to make a further study on the computational efficiency of the monic orthogonal polynomial approximation-based methods, a time-consuming convergence study is conducted. As for the first three monic orthogonal polynomial approximation-based methods, the stability lobe diagram obtained by 3rdMOPAM is the closest to the ideal one, but the computational efficiency of the 3rdMOPAM is slightly lower than that of the 1stMOPAM and 2ndMOPAM. Therefore, the 3rdMOPAM is chosen for time-consuming convergence study by comparing with the benchmark 1stSDM. The radial depth of cut ratio a_e/D is set as 1, and the parameters are the same with those used in section 3.3, down milling. The comparison of the time-consuming convergence for single DOF milling model of the 1stSDM and the 3rdMOPAM is shown in Fig. 3.

It is seen form Fig. 3 that the 1stSDM takes more time than 3rdMOPAM to generate stability lobe diagrams. Accordingly, the 1stSDM will take much more time than 1stMOPAM and 2ndMOPAM to generate stability lobe diagrams. As shown in Fig. 3, the difference of computational time between the 1stSDM and 3rdMOPAM is growing as the increase of parameter n. Therefore, compared with the 1stSDM, the 3rdMOPAM will save more time than the benchmark 1stSDM as the increase of parameter n.

4.4.2 Two DOF milling model

On the basis of DIS, the stability lobe diagrams for two DOF milling model can also be obtained by using the monic orthogonal polynomial approximation-based methods. The parameters used for two DOF milling model are the same with those used in single DOF milling model and assumed to be equal in X and Y directions. The stability lobe diagrams for two DOF milling model calculated by 1stSDM with $n = 100$ are taken as the ideal results. Stability lobe diagrams for two DOF milling model obtained by 1stSDM, 1stMOPAM, 2ndMOPAM, and 3rdMOPAM are shown in Table 4.

The computational time of 1stSDM, 1stMOPAM, 2ndMOPAM, and 3rdMOPAM for two DOF milling model to obtain stability lobe diagrams is listed in Table 4. It is observed from Table 4 that the 2ndMOPAM and 3rdMOPAM take less time than 1stSDM to generate the stability lobe diagram which is identical to the ideal curve.

We also conduct a time-consuming convergence study for two DOF milling model by comparing computational efficiency of the 3rdMOPAM with that of the 1stSDM. The comparison of the time-consuming convergence for two DOF milling model of the 1stSDM and the 3rdMOPAM is shown in Fig. 4. It is seen form Fig. 4 that the difference of computational time of the 1stSDM and 3rdMOPAM is also growing as the increase of parameter n. Therefore, the computational efficiency for the two DOF milling model of the 3rdMOPAM is also higher than that of the 1stSDM.

4.5 Convergence rate analysis

To study the convergence rate of the monic orthogonal polynomial approximation-based methods, the radial depth of cut ratio is set as $a_e/D = 1$, the spindle speed is $\Omega = 5000$ rpm, and the axial depth of cuts are chosen as $a_p = 0.2$ and 0.5 mm, respectively. The system parameters are the same with that used in section 3.3. The exact eigenvalue $|\mu_0|$ is also determined by the 1stSDM with $n = 200$. The convergence rates of the 1stMOPAM, 2ndMOPAM, and 3rdMOPAM are analyzed by comparing with the benchmark 1stSDM. Figure 5 illustrates the convergences of the eigenvalues with different computational parameters n for 1stMOPAM, 2ndMOPAM, 3rdMOPAM, and 1stSDM.

As shown in Fig. 5, it is obviously found that the 1stMOPAM, 2ndMOPAM, and 3rdMOPAM all have numerical stability. The local errors of these three monic orthogonal polynomial approximation-based methods converge to a constant eventually. The convergence rate of 1stMOPAM is the same with that of 1stSLPAM and 1stSCPAM, because the state transition matrix Ψ for the dynamic system over one period T of the 1stMOPAM, 1stSLPAM, and 1stSCPAM are same. The 2ndMOPAM has higher rate of convergence than

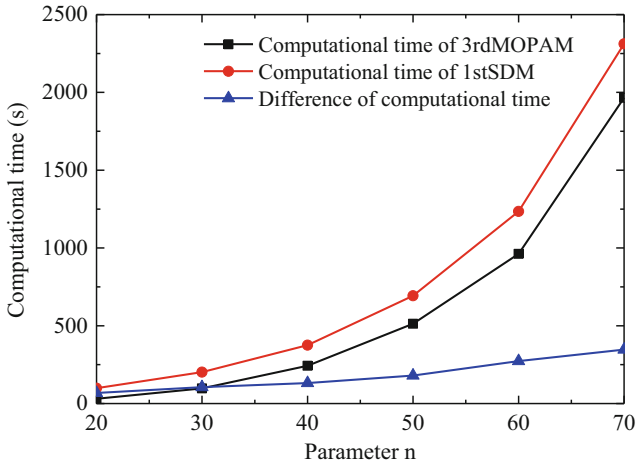

Fig. 4 Comparison of the time-consuming convergence for two DOF milling model of the 1stSDM and the 3rdMOPAM

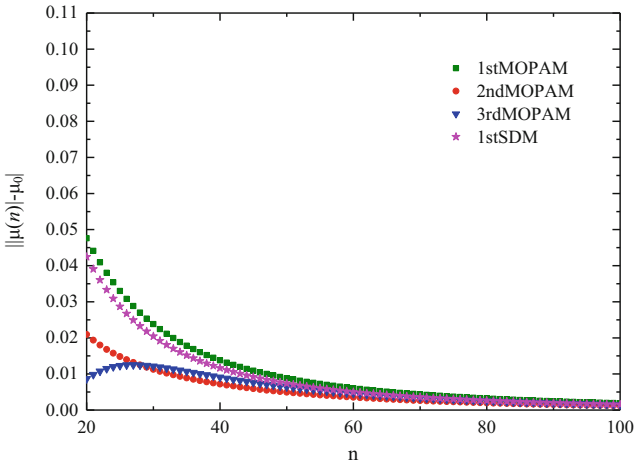

(a) a_p=0.2 mm, $|\mu_0|$=0.81923867 (stable)

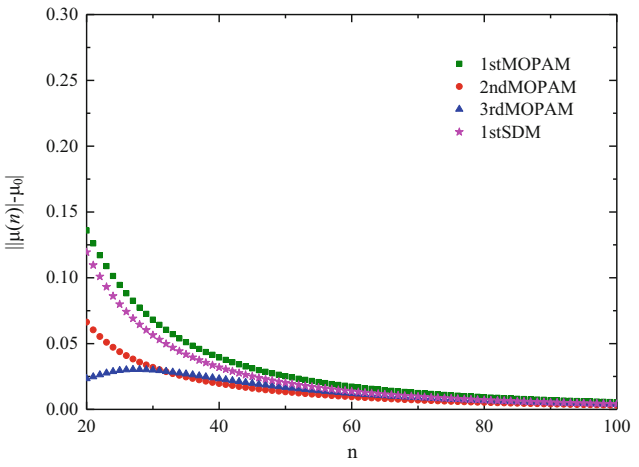

(b) a_p=0.5 mm, $|\mu_0|$= 1.07260456 (unstable)

Fig. 5 Convergence rate comparisons of 1stMOPAM, 2ndMOPAM, 3rdMOPAM, and 1stSDM. **a** $ap = 0.2$ mm, $|\mu 0| = 0.81923867$ (stable). **b** $ap = 0.5$ mm, $|\mu 0| = 1.07260456$ (unstable)

that of the benchmark 1stSDM, because the local approximation errors calculated by 2ndMOPAM are less than those of the 1stSDM; otherwise, the 2ndMOPAM converges faster than 1stSDM to a constant. As for 3rdMOPAM, it converges faster than 2ndMOPAM to a stable state, which indicates that the convergence rate of 3rdMOPAM is higher than that of the 2ndMOPAM.

Here, the convergence rate of 3rdMOPAM is higher than that of the 2ndMOPAM, and the convergence rate of 2ndMOPAM is higher than that of the 1stMOPAM. The hyper-third-order monic orthogonal polynomial approximation methods may result in higher convergence rate, but these methods also lead to more computational cost. Besides, much higher order methods may cause Runge phenomenon. As a consequence, the 3rdMOPAM can meet the requirement for high-performance milling process.

Compared with the Legendre and Chebyshev approximation-based methods, the monic orthogonal polynomial approximation-based methods have numerical stability as well as the high rate of convergence. Recently, Guo et al. [22] modified the third order FDM to predict the stability lobes for non-uniform helix tools. Similarly, the proposed monic orthogonal polynomial approximation-based methods can also be developed to analyze the stability lobes with multiple delays on the basis of DIS.

5 Conclusions

This paper focuses on the prediction of milling stability with orthogonal polynomials. The mathematical models of single DOF and two DOF milling process take regenerative effect into account. Different kinds of orthogonal polynomials are employed to analyze the milling stability. The following conclusions can be drawn.

(1) The dynamic models of single DOF and two DOF milling preocess are established. The dynamic equation of milling process is represented as DDEs in state space form.

(2) The classical Legendre and Chebyshev polynomials are utilized to approximate the state term $\mathbf{x}(s)$, delayed term $\mathbf{x}(s\text{-}\tau)$ and periodic-coefficient matrix $\mathbf{B}$(s). Then, the state transition matrix $\boldsymbol{\psi}$ is obtained by solving the DDEs based on DIS. Combining the eigenvalue of matrix $\boldsymbol{\psi}$ and the Floquet theory, the stability lobe diagrams for single DOF and two DOF milling models are generated. With the aim of evaluating the numerical stability and the convergence rate of the Legendre and Chebyshev polynomial-based methods, the 1stSDM is taken as the benchmark for comparing with these methods. The comparison results show that the numerical stabilities of the Legendre and Chebyshev polynomial-based methods need to be improved. In addition, the convergence rates of these methods are sensitive to the parameter n.

(3) In order to develop the methods that have both numerical stability and high convergence rate. The monic orthogonal polynomials are constructed to approximate the state term $\mathbf{x}(s)$, delayed term $\mathbf{x}(s\text{-}\tau)$, and periodic-coefficient matrix $\mathbf{B}(s)$. To demonstrate the computational accuracy of the monic orthogonal polynomial-based methods, the comparison between these methods and 1stSDM is conducted. The comparison results illustrate that the convergence rates of 2ndMOPAM and 3rdMOPAM are higher than that of the benchmark 1stSDM. In addition, the numerical stabilities of the monic orthogonal polynomial approximation-based methods are admirable.

(4) The stability lobe diagrams of 1stMOPAM, 2ndMOPAM, 3rdMOPAM, and 1stSDM are obtained based on Floquet theory. The comparison results show that the stability charts calculated by 2ndMOPAM and 3rdMOPAM are much closer to the ideal stability lobe diagrams. Furthermore, the monic orthogonal polynomial approximation-based methods are advantageous in terms of computational efficiency. The difference of computational time between 1stSDM and 3rdMOPAM is growing as the increase of parameter n, and the 3rdMOPAM will save more time than the benchmark 1stSDM as the increase of parameter n.

Acknowledgements This work was partially supported by the National Natural Science Foundation of China (Grant No. 51375055 and No. 51575050).

References

1. Altintas Y (2000) Manufacturing automation: metal cutting mechanics, machine tool vibrations, and CNC design. Cambridge University Press, Cambridge
2. Quintana G, Ciurana J (2011) Chatter in machining process: a review. Int J Mach Tools Manuf 51(5):363–376. doi:10.1016/j.ijmachtools.2011.01.001
3. Altintas Y, Budak E (1995) Analytical prediction of stability lobes in milling. CIRP Ann-Manuf Techn 44(1):357–362. doi:10.1016/S0007-8506(07)62342-7
4. Merdol SD, Altintas Y (2004) Multi frequency solution of chatter stability for low immersion milling. J Manuf Sci Eng 126(3):459–466. doi:10.1115/1.1765139
5. Shorr MJ, Liang SY (1996) Chatter stability analysis for end milling via convolution modeling. Int J Adv Manuf Technol 11(5):311–318. doi:10.1007/BF01845689
6. Li HZ, Li PX, Chen Q (2003) A novel chatter stability criterion for the modeling and simulation of the dynamic milling process in the time domain. Int J Adv Manuf Technol 22:619–625. doi:10.1007/s00170-003-1562-9
7. Tangjitsitcharoen S, Pongsathornwiwat N (2013) Development of chatter detection in milling processes. Int J Adv Manuf Technol 65:919–927. doi:10.1007/s00170-012-4228-7

8. Bayly PV, Halley JE, Mann BP, Davies MA (2003) Stability of interrupted cutting by temporal finite element analysis. J Manuf Sci Eng 125(2):220–225. doi:10.1115/1.1556860
9. Butcher EA, Bobrenkov OA, Bueler E, Nindujarla P (2009) Analysis of milling stability by the Chebyshev collocation method: algorithm and optimal stable immersion levels. J Comput Nonlinear Dynam 4(3):031003. doi:10.1115/1.3124088
10. Xie QZ (2016) Milling stability prediction using an improved complete discretization method. Int J Adv Manuf Technol 83(5–8):815–821. doi:10.1007/s00170-015-7626-9
11. Insperger T, Stépán G (2004) Updated semi-discretization method for periodic delay-differential equations with discrete delay. Int J Numer Meth Eng 61(1):117–141. doi:10.1002/nme.1061
12. Insperger T, Stépán G, Turi J (2008) On the higher-order semi-discretizations for periodic delayed systems. J Sound Vib 313(1–2):334–341. doi:10.1016/j.jsv.2007.11.040
13. Ding Y, Zhu LM, Zhang XJ, Ding H (2010) A full-discretization method for prediction of milling stability. Int J Mach Tools Manuf 50(5):502–509. doi:10.1016/j.ijmachtools.2010.01.003
14. Ding Y, Zhu LM, Zhang XJ, Ding H (2010) Second-order full-discretization method for milling stability prediction. Int J Mach Tools Manuf 50(10):926–932. doi:10.1016/j.ijmachtools.2010.05.005
15. Ding Y, Zhu LM, Zhang XJ, Ding H (2011) Numerical integration method for prediction of milling stability. J Manuf Sci Eng 133(3):031005. doi:10.1115/1.4004136
16. Liang XG, Yao ZQ, Luo L, Hu J (2013) An improved numerical integration method for predicting milling stability with varying time delay. Int J Adv Manuf Technol 68:1967–1976. doi:10.1007/s00170-013-4813-4
17. Quo Q, Sun YW, Jiang Y (2012) On the accurate calculation of milling stability limits using third-order full-discretization method. Int J Mach Tools Manuf 62:61–66. doi:10.1016/j.ijmachtools.2012.05.001
18. Ozoegwu CG (2014) Least squares approximated stability boundaries of milling process. Int J Mach Tools Manuf 79:24–30. doi:10.1016/j.ijmachtools.2014.02.001
19. Villadsen J, Michelsen ML (1978) Solution of differential equation models by polynomial approximation. Prentice-Hall, Englewood Cliffs
20. Funaro D (2008) Polynomial approximation of differential equations. Springer Science & Business Media, Berlin
21. Mercier B (1989) An introduction to the numerical analysis of spectral methods. Springer-Verlag New York Inc, New York
22. Guo Q, Jiang Y, Zhao B, Ming P (2016) Chatter modeling and stability lobes predicting for non-uniform helix tools. Int J Adv Manuf Technol (on line). doi:10.1007/s00170-016-8458-y